IDENTIFYING SALINIZATION THROUGH MULTISPECTRAL BAND ANALYSIS:
LAKE URMIA, IRAN

By

Danielle E. Mitchell

A major research paper
presented to Ryerson University
in partial fulfilment of the
requirements for the degree of
Master of Spatial Analysis (MSA)

Toronto, Ontario, Canada

Authors Declaration

I hereby declare that I am the sole author of this MRP. This is a true copy of the MRP, including any required final revisions.

I authorize Ryerson University to lend this MRP by photocopying of by other means, in total or in part, at the request of other institutions or individuals for the purpose of scholarly research.

I understand that my MRP may be made electronically available to the public.

Abstract

Lake Urmia, located in the Iranian provinces of West and East Azerbaijan, has been gradually, yet dramatically shrinking since the late 20th century. Surface water fluctuation up until the late 1990's never caused any reason for alarm. Since 1998, Lake Urmia has lost a devastating amount of water. Reasons for the lakes demise have been related to climate change and poor water resource management practices within the lakes watershed. If predictions of total drought become a reality, millions of people living within the Lake Urmia watershed will be faced with life altering environmental conditions. A remote sensing based analysis of multispectral imagery was used to identify changes in key features (lake water, saline features and agricultural land) and analyze the magnitude of salinization over space and time. Landsat 5 (1990, 1998, and 2006) and Landsat 8 (2013) images (acquired from USGS Earth Explorer) were analyzed at approximately 8 year intervals between 1990 and 2013. Spectral bands from the visible and near-infrared (VNIR) range were used to classify features; with the additional inputs of the thermal infrared (TIR) and Tasselled Cap Transformation (TCT) bands to highlight the reflectiveness of features. Change detection analysis of the results highlighted an alarming surface water decrease and expansion of saline features during the analysis period. From 1998 to 2013: water area decreased by 3146 km² from a maximum extent of 4995 km² to 1849 km², saline features increased by 898 km² to cover an area of 1022 km² from 124 km² and vegetation cover increased from 1159 km² to 1656 km².

Acknowledgements

Table of Contents

List of Tables

List of Figures

List of Acronyms

DEM: Digital Elevation Model

DN: Digital Number

GIS: Geographic Information System

ISODATA: Iterative Self-Organizing Data Analysis Technique

MS: Multispectral

NIR: Near Infrared

OLI/TIRS: Operational Land Imager/ Thermal Infrared Sensor

RA: Risk Analysis

SD: Standard Deviation

TCT: Tasselled Cap Transformation

TIR: Thermal Infrared

TM: Thematic Mapper

TOA: Top of Atmosphere

UNDP: United Nations Development Programme

UNESCO: United Nations Educational, Scientific and Cultural Organization

USGS EE: United States Geological Survey Earth Explorer

VNIR: Visible and the Near Infrared

WRS-2: World Reference System 2

CHAPTER ONE: Introduction

One of many adverse environmental impacts of a shrivelling water cycle is the process and presence of salinization. Saline environments can result from naturally occurring (product of primary salinity), or human-induced (secondary salinity) processes (Allbed and Kumar, 2013). Of greatest concern to environmental scientists are the nature of anthropogenic activities that directly or indirectly contribute to rising concentrations, and the distribution of saline evaporites. Causes of salinization are commonly attributed to irrigation practices, industrial pollutants, as well as infrastructure related to urban growth and resource extraction (Podmore, 2009).

Water volume loss occurs during dry, drought-like conditions. As saline water evaporates, salt particles are precipitated onto the shoreline. When exposed on bare land, saline minerals can be transported in windstorms and deposited elsewhere. Salt storms cause intolerable air quality conditions for people, animals, vegetation and infrastructure (Pengra, 2012). Inhaling suspended saline particles has been attributed to cases of esophagus cancer, respiratory disease and birth defects reported in the Middle East (Pengra, 2012). Transporting saline evaporites into intolerant ecosystems can fatally impact fragile crops and vegetation. As well, the abrasive nature of wind-transported saline particles can cause physical or chemical erosion to the exterior of buildings or infrastructure. Salt storms, similar to sand storms, can move suspended saline particles around a radius of 500 km from the storms start point (Garousi *et al.,* 2013). Damage from the resulting salt deposits has harmful effects on the local environment and in surrounding regions. Neighbouring countries to Iran, including Turkey, Iraq, Azerbaijan and Armenia may also experience the devastating effects of salt storms (Garousi *et al.,* 2013). This may induce trans-border environmental hazards, pose questions of responsibility for the source of environmental degradation, and raise concerns of environmental justice.

1.1 Image Analysis of Remote Environments

Satellite imagery provides means of interpreting and monitoring environmental conditions, without the cost, difficulties or time consuming nature of fieldwork. Isolated environments are typically under surveyed and are poorly represented by spatial data. In some cases, where little fieldwork has been done, geographic data are limited to satellite and aerial imagery. This is not to say that remote environments are necessarily distant from populous city centres. Acquisition and accessibility of spatial data and imagery can be limited, or non-existent for political or economic reasons; therefore an otherwise urbanized environment is poorly represented by geospatial data, resembling the analytic limitations of remote environments (Eimanifar and Mohebbi, 2007).

1.2 Study Area

Lake Urmia, located in northwestern Iran, lies on the border of East and West Azerbaijan Provinces (Figure 1.1) in the Turkish-Iranian Plateau. The lake is situated at the intersection of the Armenian Highlands and the Iranian Plateau. Four mountain ranges surround Lake Urmia; Caucasus Mountains (north) Sami Dagi Mountains (west), Zagros Mountains (south) and the Elburz Mountains (east) (DeLorme, 2012; Esri, 2012; NPS, 2012; USGS, 2012; Google Earth, 2013).

Northern Iran is situated amongst numerous climate classifications, according to the Köppen-Geiger model, but is typically referred to as a semi-arid or steppe environment (Christopherson and Bryne, 2009). Figure 1.2 displays the average monthly temperature (°C) and precipitation (mm) for the City of Urmia between 1990 and 2009 (World Bank, 2014). Yearly evaporation at Lake Urmia is modelled at 1020mm/year by (Zeinoddini *et al.,* 2014).

Figure 1.1: (left) Lake Urmia located in northwestern Iran, (right) separated by the border of West and East Azerbaijan and capital cities of Urmia and Tabriz respectively (Source: Google Earth, 2013).
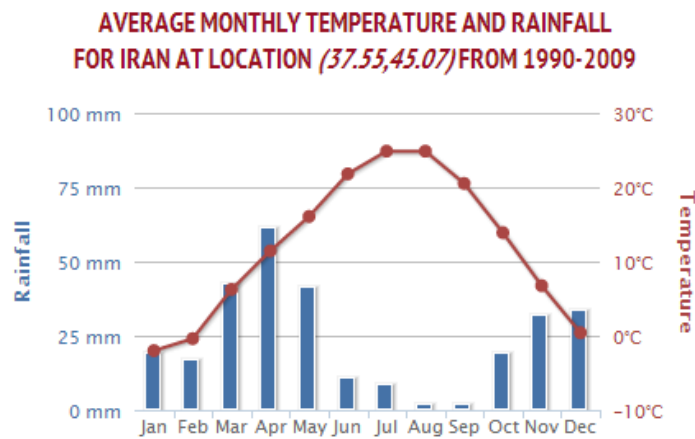
Figure 1.2: 1990 to 2009 average monthly temperature (°C) and precipitation (mm) counts (World Bank, 2014)

Lake Urmia is characteristically a hypersaline, endorheic lake with salinity levels measured at 300g/L in 2012 (Pengra, 2012). From a surface size of 6,100 km² in 1995 to 2,366 km² in 2011, the lakes salinity has surpassed sustainable concentrations for brine tolerant species in a saline environment (Pengra, 2012). The lakes shrinking size has been attributed to climate

3

change (Abbaspour *et al.,* 2012), poor water management (Garousi *et al.,* 2013), the construction of a pipeline to Tabriz (Khalyani *et al.,* 2014) and the Lake Urmia Causeway (Kabiri *et al.,* 2012). The pipeline was built in 1999 to withdraw 3 billion m³ of water from the Lake Urmia watershed to the capital city of Tabriz (Khalyani *et al.,* 2014). Construction of the causeway took approximately 30 years and was completed in 2008 (Khalyani *et al.,* 2014). Built as a solid 16 km embankment, a single opening measuring 1.25 km near the centre of the causeway allows limited flow from the now divided north and south portions of the lake (Khalyani *et al.,* 2014). The purpose of this bridge was to foster better communication and transportation between the highly urbanized, and densely populated capitals of West Azerbaijan (Urmia City) and East Azerbaijan (Tabriz) (Zarrineh and Azari Najaf Abad, 2014).

Water loss and increasing salinity within the environment is causing the Lake Urmia ecosystem to collapse. Migratory flamingos can no longer feed in Lake Urmia due to high salinity depleting their food source (brine shrimp), and causing them physical harm (Pengra, 2012). Consequently, ecosystem degradation impacts the economic value of the lake by diminishing one of its single most profitable and admirable natural attractions. Increasing salinity throughout the extent of Lake Urmia's drying lake basin is also posing health concerns related to air quality (Garousi *et al.,* 2013). Lake Urmia services 76 million people within its watershed (Pengra, 2012) of which, 6.4 million rely on the freshwater inputs to the southern portion of the lake for irrigation and agriculture (Zeinoddini *et al.,* 2014).

1.3 Research objectives

The purpose of this study is to illustrate and quantify environmental degradation and risks associated with the relative rate of evaporation and salinization of Lake Urmia. Overall water loss is visible in unaltered remotely sensed images (Figure 3.1) yet a change detection analysis will represent the trajectory of pixel classification over time. Three time periods were chosen, based on available imagery from the United States Geological Survey Earth Explorer (USGS EE), in

which change detection analysis will be conducted; 1990 and 1998, 1998 and 2006, 2006 and 2013. The periods of analysis created encompass times of natural lake fluctuation prior to 1998 (Zarrineh and Azari Najaf Abad, 2014) leading to unnatural water loss from resource extraction to present day (Pengra, 2012). This study attempts to analyze how select features (*Water, Saline Features,* and *Vegetation*) change over time.

CHAPTER TWO: Literature Review

2.1 Conservation Initiatives and Strategies

In 1971, Lake Urmia was identified under the Ramsar Convention as a *Wetland of International Importance*, as well as a Biosphere Reserve in 1976 by the United Nations Educational, Scientific and Cultural Organization (UNESCO) (Pengra, 2012). Currently, the United Nations Development Program (UNDP) recognizes two functioning environmental management groups, encompassing government, non-government organizations, and members of the public as the *National Committee for Sustainable Management of Lake Urmia* and the *Regional Council for Management of Lake Urmia Basin.* In 2010, the *Integrated Management Plan for Lake Urmia Basin* was presented via the joint Conservation of Iranian Wetlands Project with the United Nations Environmental Program (UNEP), Global Environmental Facility, and the Department of Environment (Eimanifar and Mohebbi, 2007). Projected over 25 years (commencing in 2010), three management goals are set for the conservation and management of Lake Urmia as; "'To raise awareness of the values of the lake and satellite wetlands and to enhance public participation in their management', 'Sustainable management of water resources and land use', and 'Conservation of biodiversity and sustainable use of the wetland resources'" (Ramsar, 2010). Regardless of action plans or management group creation, Eimanifar and Mohebbi (2007) have highlighted the lack of improvement in the lakes ecosystem, and have questioned the reliability of these conservation groups.

Traditional specializations in water related infrastructure could create opportunities for sustainable resource extraction when implemented appropriately (Ayboga and Ilhan, 2012; Khalyani *et al.,* 2014; Zarrineh and Azari Najaf Abad, 2014). Khalyani *et al.* (2014) suggest encouraging traditional rain-fed agricultural practices to reduce water waste from irrigation. Iran is also one of the most productive countries of damming infrastructure (Ayboga and Ilhan, 2012). With the engineering capabilities already present, Ayboga and Ilhan (2012) promote opportunities for construction of flow regulating dams, as well as creating comprehensive damming policies.

2.2 Saline Evaporites and Features

Salt and salinity is prominent in arid and semi-arid soils and endangers an already fragile environment. Saline soils and salt crusts feature recognizable textures and properties in remotely sensed imagery (Srestha and Farshad, 2009). Salt crusts like those visible along the shoreline of Lake Urmia (Figure 2.1) exhibit significant texture characteristics that allow for differentiation amongst other soil types. When using remote sensing technology to detect saline soils, the majority of findings identified saline crusts to appear texturally smoother and more reflective (in the visible- near infrared range (VNIR)) than non-saline soils or features (Singh and Sirobi, 1994; Metternicht and Zinch, 2003; Allbed and Kumar, 2013). Depending on the predominant mineral of a salt crust, reflective properties can vary between puffy salt crusts (sodium sulphates) and smooth salt crusts (chlorides), which lead to further indications of soil salinity characteristics in the area (Driessen and Schoorl, 1973; Eghbalm *et al.,* 1989).

Figure 2.1: Salt crusts (left) along the shoreline of Lake Urmia and salt scalds (right) throughout the dry lake bed (Sources: Urmulu, 2011; Noroozi, 2014).

Common saline evaporites include but are not limited to gypsum, halite and calcium carbonate (Howari, 2002). Reflective quantity diminishes if saline crusts develop cracks (Metternicht and Zinch, 2003) or accumulate soil impurities. This is common through wind transport of sediments, vegetation or other organic matter and pollutants in continental environments (Csillag *et al.,* 1993; Farifteh *et al.,* 2006; Allbed and Kumar, 2013). Salt scalds

(Figure 2.1) are formed from the accumulation of saline minerals, forming and impermeable surface (McMullen, 2000)

2.3 Multispectral vs. Hyperspectral Imagery

Detecting and mapping features in saline environments with remotely sensed imagery has been successful through the use of both multispectral and hyperspectral imagery (Dwivedi *et al.,* 1999; Farifteh *et al.,* 2006; Weng *et al.,* 2008; Setia *et al.,* 2011; Dehni and Lounis, 2012; Koshal, 2012; Teggi *et al.,* 2012; Allbed and Kumar, 2013). Yet the limitations to both image types maintain "no agreed-on best approach to this technology for monitoring and mapping soil salinity" (Allbed and Kumar, 2013). Researchers are hesitant to use multispectral imagery for salinity mapping since low spatial resolution can cause pixel misclassification (Dehaan and Taylor, 2003; Allbed and Kumar, 2013). Dehaan and Taylor (2003) also deem "traditional classification techniques" to be a limiting factor when using multispectral data.

Undeterred by its shortcomings, multispectral imagery has been stated in the literature to be a "preferred method for mapping and monitoring soil salinity" (Dehaan and Taylor, 2003; Allbed and Kumar, 2013). Due to significantly higher resolution and more bands acquired by hyperspectral imagery, better quantitative analysis can be performed for saline soil identification (Dehaan and Taylor, 2003). However, multispectral data such as that captured by Landsat satellites are much more accessible and affordable (free downloads are available from the USGS EE) than hyperspectral images.

Imagery acquired from Landsat TM has been successfully interpreted for soil salinity and soil type identification studies, and is the most common type of imagery cited throughout numerous publications (Verma *et al.,* 1994; Goossens *et al.,* 1999; Elnaggar and Noller, 2009; Kabiri *et al.,* 2012; Allbed and Kumar, 2013). Due to the broad nature of Landsat band sensors, Dehaan and Taylor (2003), Farifteh *et al.* (2006), and Allbed and Kumar (2013) have identified potential problems of mixed pixels, poor spatial and spectral resolution as well as limitations

during transformations and classifications in their own research. To account for data limitations and accuracy, research suggests additional ancillary data inputs such as field data, geographic information systems (GIS), and digital elevation models (DEM) with multispectral images (Sah *et al.,* 1995; Eklund *et al.,* 1998; Metternick and Zinck, 2003; Allbed and Kumar, 2013).

2.4 Thermal Infrared Band

Research conducted on remote sensing of soil salinity is two-fold, related to quantitative analysis and qualitative characteristics of saline evaporites. Quantitative research on soil salinity focuses on band experimentation (Verma *et al.,* 1994; Goossens *et al.,* 1999; Allbed and Kumar, 2013), spectral (Howari, 2002) and statistical analysis (Fernandez-Buces *et al.,* 2006) of spectrum absorption and reflectance. Qualitative analysis of saline soils and salt crusts emphasize texture, efflorescence, and soil composition (Csillag *et al.,* 1993; Metternicht and Zinch, 2003; Fernandez-Buces *et al.,* 2006).

Researchers have identified how essential thermal bands and infrared spectra are to detecting and mapping soil salinity. Conventional methods of soil detection through multispectral image analysis are visualized by graphing soil reflectance (%) against wavelength (µm) (Howari, 2002). Studies that have used Landsat Thematic Mapper (TM) imagery highlight the advantages of including band 6 (thermal infrared) to differentiate between soil types and mineral compositions (Verma *et al.,* 1994; Goossens *et al.,* 1999; Allbed and Kumar, 2013). In Goossens *et al.* (1999) and Naseris (1998) studies of saline environments in Iran, the authors' additions of band 6 from Landsat TM imagery into their analysis "improved the separation of saline soils from gypsiferous and coarse-textured desert soils". Similar results were echoed in the analysis of saline soils in India, where Verma *et al.* (1994) combined visible bands (bands 1-3), near infrared (band 4) and thermal (band 6) of Landsat TM imagery to distinguish between spectrally similar saline soils.

In the visible and near-infrared portion of the electromagnetic spectrum, saline minerals are strongly reflected between 0.4 and 2.5 μm (Crowley, 1991; Schmid *et al.,* 2008; Mulder *et al.,* 2011). Throughout related literature, there is a general consensus that thermal bands are essential in remote sensing applications of saline detection for separating spectrally similar soil types (Hunt *et al.,* 1972; Mougenot *et al.,* 1993; Verma *et al.,* 1994; Goossens *et al.,* 1999; Howari, 2002; Metternicht and Zinch, 2003; Farifteh *et al.,* 2006; Allbed and Kumar, 2013). Farifteh *et al.* (2006) highlight the advantage of analyzing and detecting saline soils during periods of low vegetative growth, "for example, at the end of hot and dry season and, or when high percentage of bare soil is available". The electrical conductivity of saline soils, like those including sulphates, phosphates, chlorides, carbonates of sodium, calcium, magnesium, gypsum and halite evaporites are found to be strongly related to near infrared (NIR), mid-infrared (MIR) and thermal infrared (IR) spectra (Siegal and Gillespie, 1980; Metternicht and Zinck, 2003; Shrestha, 2006; Metternicht and Zinck, 2010; Mulder *et al.,* 2011). Shrestha's (2006) study of electrical conductivity of soil properties in Thailand utilized Landsat TM bands 1 through 5 and 7, with the addition of band 6 for its well-known capabilities to differentiate between spectrally similar saline soils (Verma *et al.,* 1994). Overall, soil salinity research stresses the importance of thermal band input for soil differentiation, and the electric, chemical and physical characteristics of evaporative minerals.

2.5 Tasselled Cap Transformation

The Tasselled Cap Transformation (TCT) has been previously used in remote sensing studies of saline environments (Peng, 1998; Metternick and Zinck, 2003; Masoud and Koike, 2006; Elnagger and Noller, 2009). The TCT is generally understood to identify brightness, greenness and wetness (or yellowness) of pixels in an image (Kauth and Thomas, 1976). The initial purpose of the wetness band was to report soil moisture (Crist and Cicone, 1984); however Scott *et al.* (2003) suggest, "…the wetness component is exploited to differentiate land from

water". Additionally, the brightness band can be used to identify saline soils from their highly reflective characteristics (Peng, 1998). Relative to the image classification process, Masoud and Koike (2006) found the TCT to enhance the detection and classification of saline features.

CHAPTER THREE: Data and Methodology

3.1 Image Acquisition and Preprocessing

Landsat images were acquired from the Landsat Archive available through the USGS EE webpage (http://earthexplorer.usgs.gov). Table 3.1 outlines their characteristics and provides identifiers for each scene. Lake Urmia is located at the intersection of Landsat World Reference System 2 (WRS-2) path 169 and row 34. In each image, the lake is situated in the northeast corner where, in some cases, sections of the lake were not captured by the satellite. Mosaicking multiple images to cover the entire lake was beyond the scope of this project. To account for this problem all images were clipped to the same extent, an area of 16,705 km², eliminating any discrepancies between years. From Landsat 5 Thematic Mapper (TM) three images were acquired for the years 1990, 1998 and 2006. The most recent Landsat image was acquired from the Landsat 8 Operational Land Imager (OLI) and Thermal Infrared Sensor (TIRS) for the year 2013.

Table 3.1: Characteristics and identifiers of acquired Landsat images from the USGS EE website.

Satellite	Acquisition Date	Landsat Scene ID	Resolution	Cloud Cover
Landsat 5 (TM)	**1990/08/19** 06:58:33	LT51690341990231XXX06	30m	0.00%
	1998/08/25 07:17:11	LT51690341998237AAA01	30m	0.00%
	2006/09/16 07:32:24	LT51690342006259MOR00	30m	0.00%
Landsat 8 (OLI/TIRS)	**2013/09/19** 07:40:33	LC81690342013262LGN00	15m, 30m, 100m	4.97%

a)   b)

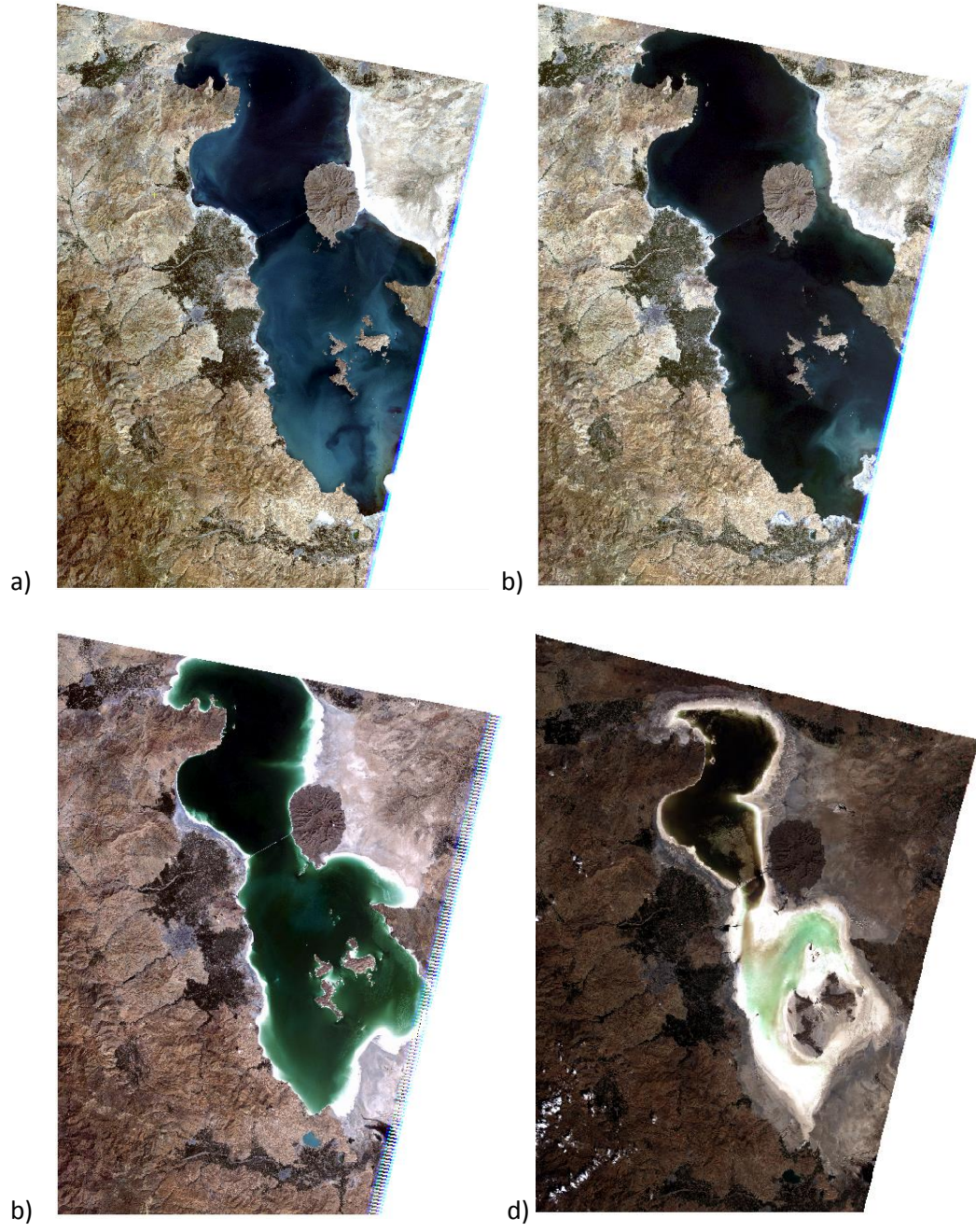b)   d)

Figure 3.1: Natural Colour Landsat images of Lake Urmia; a) 1990, b) 1998, c) 2006, d) 2013

Prior to acquisition, the images listed above were preprocessed to Standard Precision and Terrain Correction, denoted Level 1T. By doing so, the imagery acquired by the user has already undergone topographic correction processes that relate ground control points to digital elevation models (DEM). Additional corrections were made to convert the original pixel values from digital numbers (DN) to physical reflectance. By correcting images to Top of Atmosphere (TOA) reflectance, temporal data comparisons between images will not be affected by differing atmospheric conditions at the time of acquisition (PCI, 2010). An issue that presented itself with TOA correction was its removal of thermal infrared bands from the image data. Thermal bands cannot be corrected to reflectance measures through TOA correction, however the literature on remote sensing of saline environments highly recommends the use of the thermal band in Landsat imagery for salt detection (Verma *et al.,* 1994; Goossens *et al.,* 1999; Allbed and Kumar, 2013). Therefore the thermal band was transferred back into TOA corrected images for analysis.

Among the four images selected, three time periods were defined, each representing change covering approximately 8 years. The purpose of creating three time frames is to account for natural fluctuation in lake surface area up to 1998, as noted by the UNEP (Pengra, 2012). Saline features are reported to be most prominent during the dry season in semi-arid climates (Farifteh *et al.,* 2006). In Iran, August and September are the driest months of the year, averaging less than 3mm of precipitation per month (Figure 1.2). The most recent time frame of 2006 and 2013 will only represent change in the environment over a 7-year period; due to the fact that imagery from August/September 2014 is not yet available.

3.2 Image Classification

The combination of input bands was selected to highlight three key features during the classification process: *Water* (exclusively Lake Urmia), *Vegetation* (ideally agricultural land identified by its geometric shape), and *Saline Features* (including saline evaporates, highly saline

soils and salt scalds). Table 3.2 displays characteristics of each spectral band, or image transformation output used for classification purposes.

Table 3.2: Spectral band and band transformation used for the image classification process.

Band	Band No. L5/L8	Band Information
Blue	1/2	Effective at identifying differences in bare soil and vegetative environments. Best band for water penetration (Quinn, 2001; USGS, 2014)
NIR	4/5	Useful for differentiating between feature boundaries based on moisture; land/water boundaries, dry/wet soils, vegetation/bare land (Quinn, 2001; USGS, 2014)
TIR	6/10	Thermal bands are proven to be essential in remote sensing of soil salinity for their electromagnetic responsiveness (Verma *et al.,* 1994; Goossens *et al.,* 1999; Allbed and Kumar, 2013)
TCB	Tasselled Cap Brightness	Captures highly reflective features such as bare soil, urban or man-made environments (ArcGIS Help, 2014)
TCW	Tasselled Cap Wetness	Highlights moisture within the image. Degrees of soil moisture and water features (ArcGIS Help, 2014)

Unsupervised classification method was selected over supervised classification for two key reasons. Supervised classifications require the user to identify features by manually creating training areas. Without additional reference data or imagery, it can be difficult to justify the creation of training areas representing each feature classification. The overall unfamiliarity of the environment and lack of additional reference data supported the decision to implement the unsupervised classification method. Selecting the optimum classification algorithm was an experimental process. There are three classification algorithms in the PCI Geomatica software to select when conducting an unsupervised image classification: K-Means, Fuzzy K-Means, and ISODATA. The K-means algorithm was immediately dismissed as an option for classifying imagery of Lake Urmia. This is due to the fact that the Fuzzy K-Means and ISODATA algorithms provide better classification of mixed pixels when they are run according to iteration parameters set by the user (Yale, 2001; *Chang et al.,* 2011). Fuzzy K-Means is described as a softer approach to k-means clustering where pixels can be classified by a "degree of belongingness" to cluster centres (Chang *et al.,* 2011). This method requires the user to determine a fixed number of total classes before the classification is run. The Iterative Self-Organizing Data

Analysis Technique (ISODATA) does not require the user to determine a fixed number of classes yet maintains the fuzzy characteristics of the Fuzzy K-means algorithm. Instead, ISODATA simply requires the user to conceive parameters such as the maximum and ideal number of classes, and then the algorithm itself determines the actual number of classes. The ISODATA algorithm requires the user to trust the iterative process when classifying pixels. At the same time, it limits parameter experimentation required in both k-means and fuzzy k-means when determining the minimum and maximum number of classes to be created (Memarsadeghi *et al.,* 2007). For the unsupervised classification of all four Lake Urmia images, the algorithm parameters were set as follows: Minimum Clusters – 2, Maximum Clusters – 50, Desired Clusters – 30, Maximum Iterations – 25, and the remaining parameters were left at their default values. Cluster limits were set after conducting an ISODATA classification with default parameters then, experimenting with various combinations of clusters until meaningful groupings were maximized. The result of the unsupervised classification by ISODATA algorithm produced 40 classes for each image.

3.3 Post Classification Analysis

An accuracy assessment was conducted upon completion of the class aggregation process. This assessment overlays 300 random points onto each classified image (Forsythe and McCartney, 2014), then prompts the user to reclassify each random point from a reference image. The rule of thumb when creating random sampling points is to use 50 points per feature class (Congalton, 1991). The number of random sampling points were increased to 300 for 4 feature classes to account for the feature size within the image, and the chance that a random sampling point will not actually represent a narrow or scattered feature.

The output of an accuracy assessment is an Error (Confusion) Matrix as well as an Accuracy Report. The diagonal of the Error Matrix represents the random points that were correctly identified by the reference image as the same class in the classified image. Pixel values

listed outside of the diagonal report misclassified pixels between the reference and classified images. The accuracy statistics report breaks down class accuracy by Producers Accuracy and User Accuracy. Producer's Accuracy represents errors of omission within the data meaning the percent of pixels accurately classified in the reference image (Congalton, 1991). Errors of omission represent the percent of pixels that failed to be classified into its appropriate classification (Congalton, 1991). This statistic represents the ability to accurately classify pixels from the reference data. User Accuracy represents the reliability of the classified data to actually represent the same feature class in real life. Kappa statistics are calculated as a measure of agreement between the producer and user accuracies, otherwise described as "the agreement between model predictions and reality" (Lentilucci, 2006). This statistic depicts the likelihood of pixels being classified correctly by chance. The remote sensing community advocates that when k $= > 0.8$ it is unlikely that classification was due to chance. When k $= < 0.4$ it is understood that there is a greater disagreement between a pixels representation and predicted class, therefore more likely classified due to chance (Lentilucci, 2006). Therefore Kappa statistics greater than 80% will be interpreted as an accurate classification of pixels into the three feature classes of *Water, Saline Features* and *Vegetation.*

3.4 Image Band Differencing

Band differencing is the process wherein temporal change between two images at the same location is calculated by subtracting the same bands in each image from each other. Essentially this calculation creates an output image depicting "change" and "no change" in the environment from a single band. To detect feature change over time at Lake Urmia, a band differencing image was created by subtracting NIR bands of the older image from the newer image for each time period. The near-infrared band was selected for its ability to differentiate between feature boundaries (Quinn, 2001) as listed above in Table 3.2. The values created through band differencing represent no change, positive or negative change in reflectance of the

NIR band from 1990 to 1998, 1998 to 2006, and 2006 to 2013. Positive values represent pixels that have increased in reflectance over time, whereas negative values represent the opposite, where pixels have decreased in reflectance over time. Pixels assigned a value of 0 have not experienced any change. That being said, a value of 0 may not be the best representation of "no change" pixels. By applying a threshold to what are considered "no change" pixels, those which show extreme positive or negative change will be better visualized. Each output image was manually classified into 6 classes where classification breaks represent one half standard deviation (SD) from the mean. The thresholds created around the mean extended "no change pixels" to slightly more than 0, encompassing more instances of limited change over time, highlighting greater change further from each mean.

3.5 Image reclassification

Classes in both the aggregation and band differencing images were reclassified in order to create a meaningful change detection legend. Table 3.3 outlines how classes were numerically reclassified, and then explains the output values from raster calculation in the final change detection images.

Table 3.3: Image reclassification values, raster calculation output values and their meanings

Band Differencing Image Number = Class	Aggregate Image Number = Class	Calculation Output (Raster addition)	Output Interpretation
100 = No Change	1 = *Water*	101	No Change, *Water*
200 = Negative Change	2 = *Other*	102	No Change, *Other*
300 = Positive Change	3 = *Vegetation*	103	No Change, *Vegetation*
	4 = *Saline Features*	104	No Change, *Saline Features*
		201	Growth of *Water*
		202	Loss of *Other*
		203	Loss of *Vegetation*
		204	Loss of *Saline Features*
		301	Loss of *Water*
		302	Growth of *Other*
		303	Growth of *Vegetation*
		304	Growth of *Saline Features*

Again, "no change" pixel classification contains pixels with little to no change in reflectance within a half standard deviation from the mean. "Positive change" identifies pixel clusters that have increased ("growth") in reflectiveness over time, whereas "negative change" represents clusters of pixels that have decreased ("loss") in reflectiveness over time. From here, visual interpretation of the change detection classes will prompt a spatial analysis of feature class changes over time.

CHAPTER FOUR: Results and Analysis

4.1 Results

The unsupervised classification output presented 40 clusters from the ISODATA parameters for each of the four years. The average number of clusters aggregated to represent classified feature categories are as follows; *Water* – 5, *Vegetation* – 2.75, *Saline Features* – 9.25, and *Other* - 23. Figures 4.1, 4.2, 4.3 and 4.4 display the aggregated feature classifications for 1990, 1998, 2006 and 2013 respectively. The number of pixel clusters created to represent vegetation was the most consistent over time. Between 2006 and 2013 the number of pixel clusters identifying water doubled from 4 to 8. In contrast, the number of pixel clusters highlighting salinity decreased by approximately half between 2006 and 2013 from 12 to 7. Pixel representation became more homogeneous for *Saline Features* between 2006 and 2013, requiring fewer clusters. As the lake continues to decrease in water volume, the bathymetry of the lake itself creates sections of varying depths of water throughout the lake. Thus more clusters are created to represent the various depths of water as the identification of pixels representing Lake Urmia becomes more complex.

From the classification images alone, logical inferences can be made about the changing environment from 1990 to 1998 (Figure 4.1). As was previously identified in the literature review, severe water loss began in 1998 (Figure 4.2) continuously declining to 2013 (Figure 4.4). At the same time, aggregate classes representing *Saline Features* appear to increase in the 2006 (Figure 4.3) and 2013 classified images. The *Other and Saline Features* classifications should increase where evaporated water has exposed the lakebed and left behind evaporated salt. .

Figure 4.1: Landsat 5, 1990 aggregate feature classification where blue – *Water,* red – *Saline Features,* green – *Vegetation* and white – *Other.*

Figure 4.2: Landsat 5, 1998 aggregate feature classification where blue – *Water,* red – *Saline Features,* green – *Vegetation*, white – *Other.*
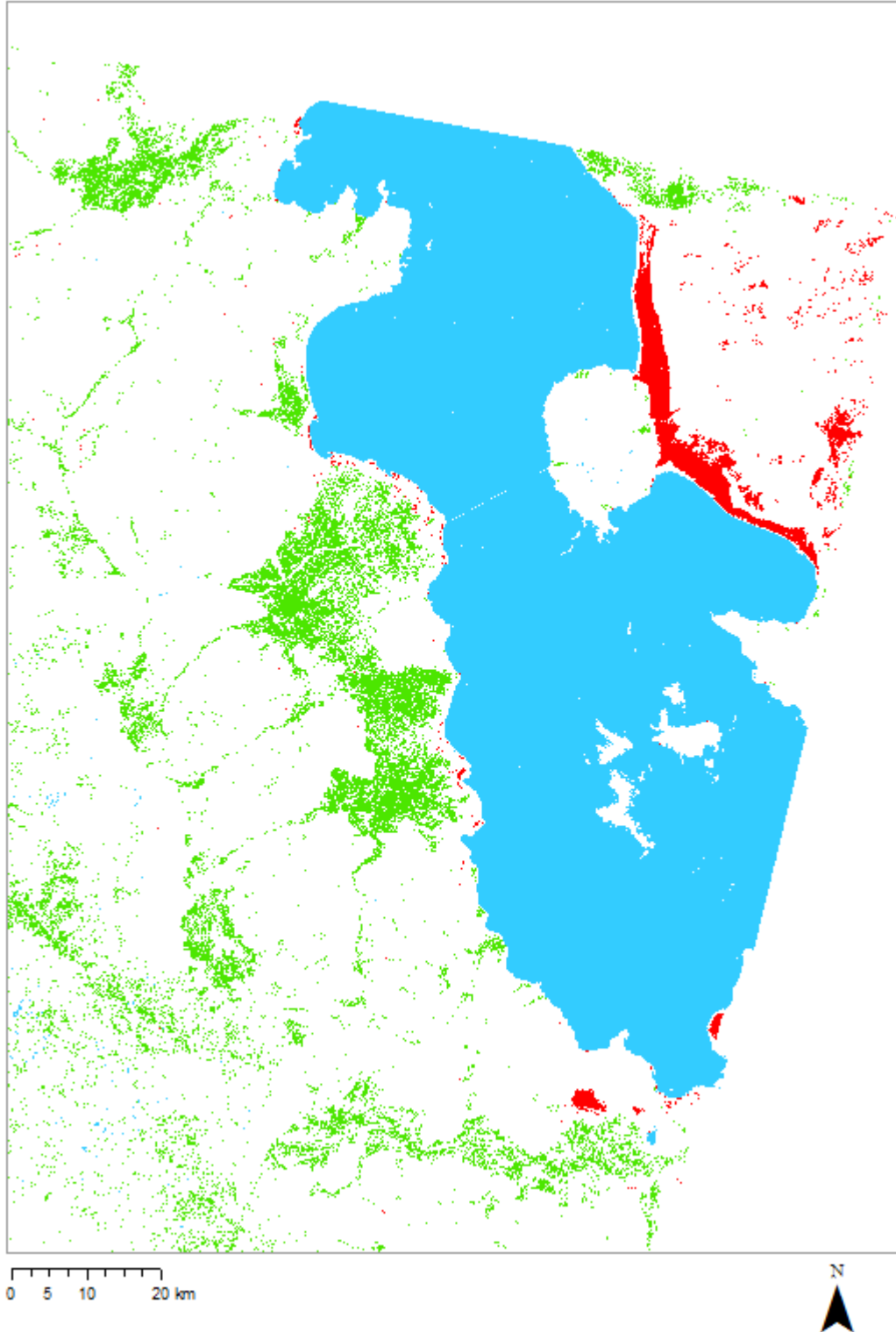
Figure 4.3: Landsat 5, 2006 aggregate feature classification where blue – *Water,* red – *Saline Features* green – *Vegetation,* and white – *Other.*
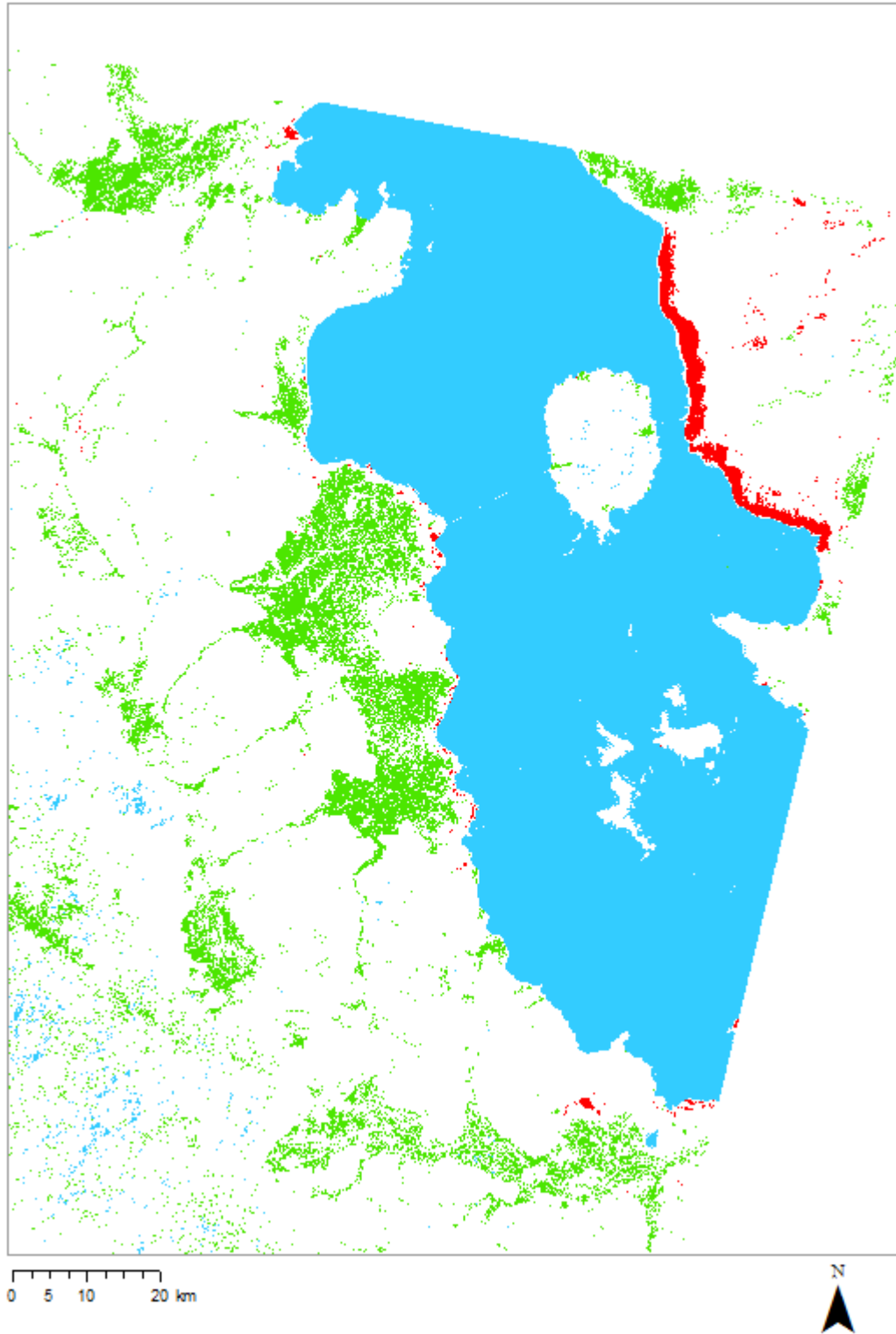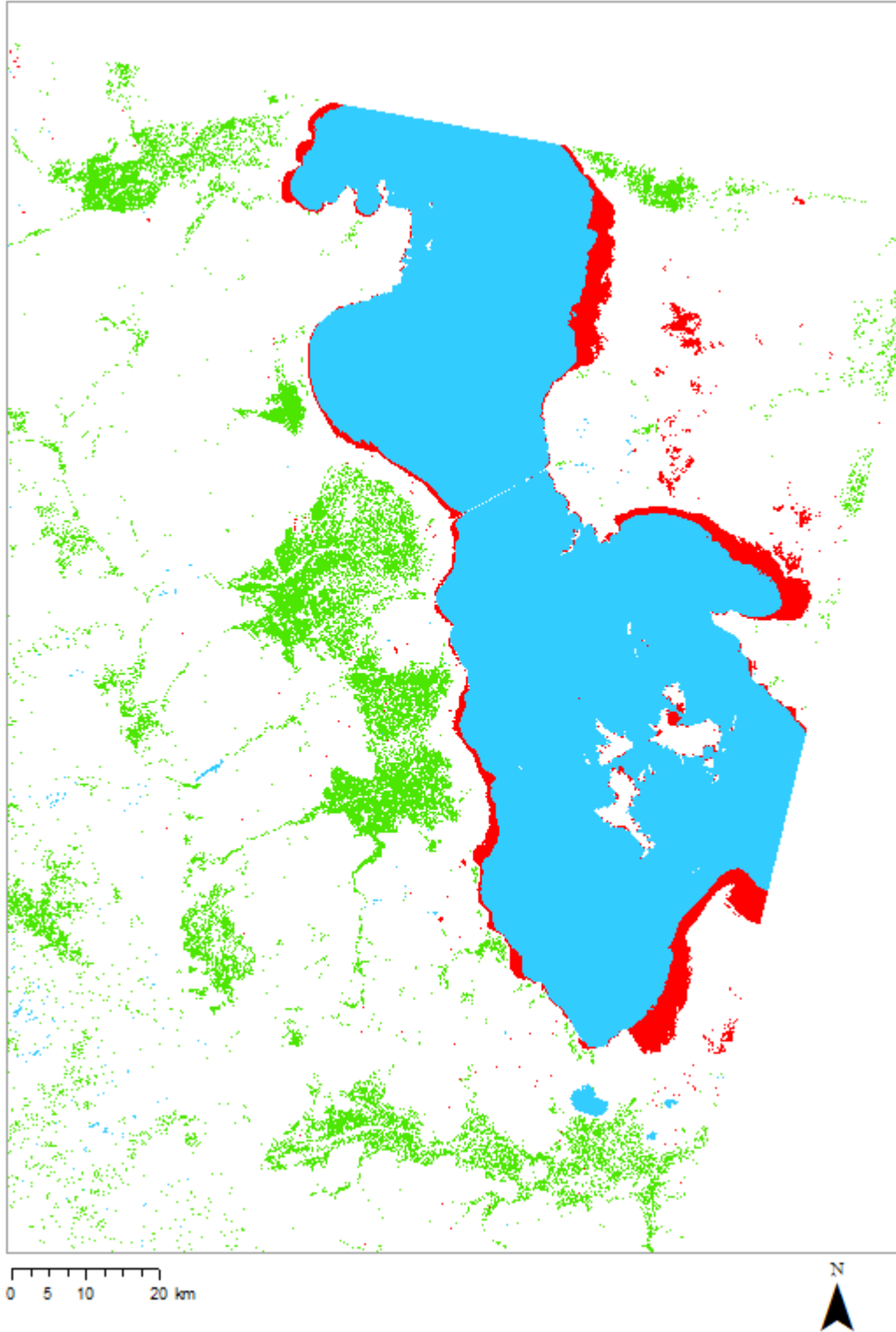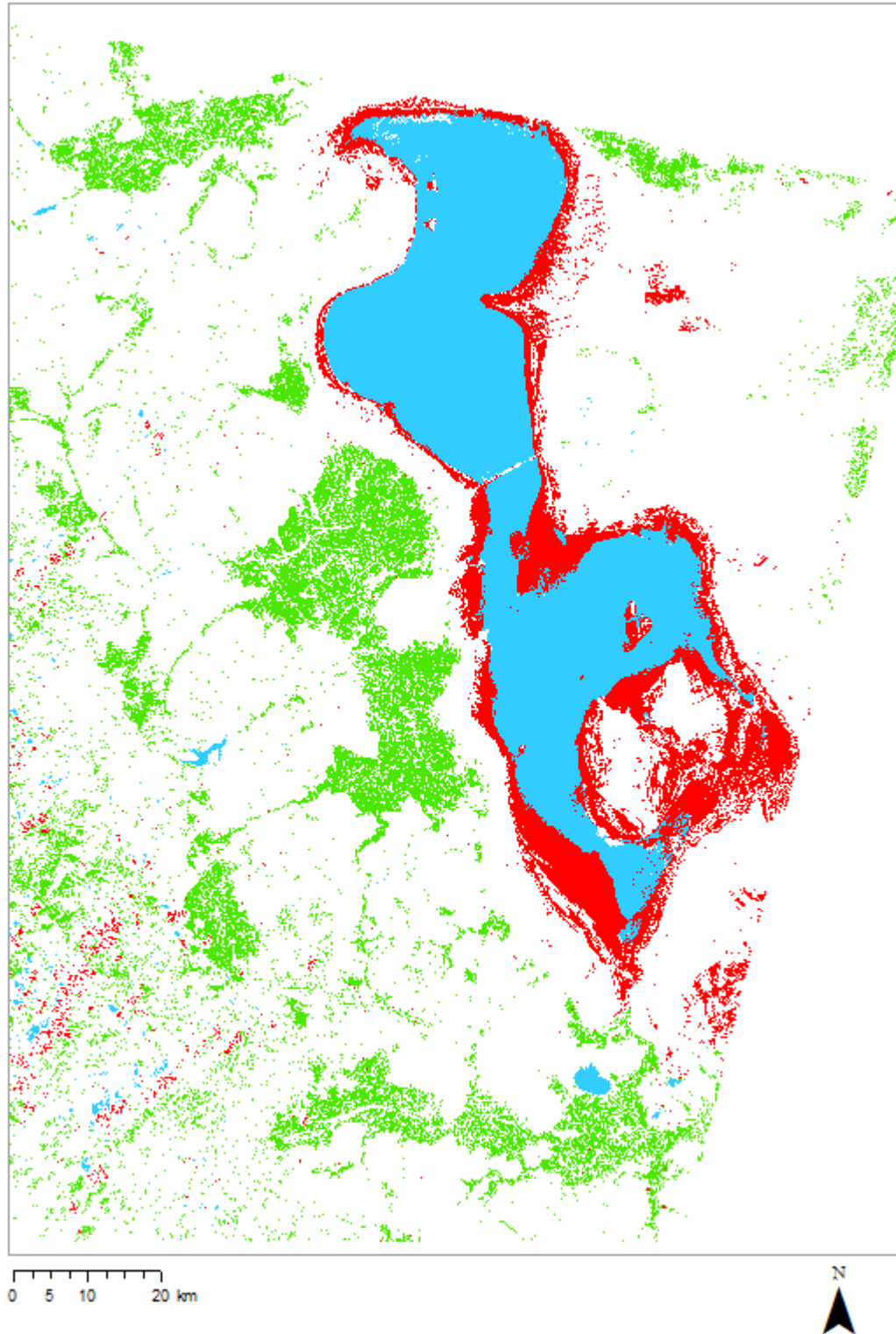
Figure 4.4: Landsat 8, 2013 aggregate feature classification where blue – *Water,* red – *Saline Features,* green – *Vegetation and* white – *Other.*

4.2 Accuracy Assessment

Accuracy assessments conducted on all images received over 90% accuracy (Figure 4.5). Kappa coefficients also all exceed the threshold of $k > 0.8$ (as defined by Lentilucci, 2006) meaning that the image classifications all have a high degree of validity. Accuracy statistics from each year do however highlight errors of omission and commission amongst pixels through the Producer and User Accuracy.
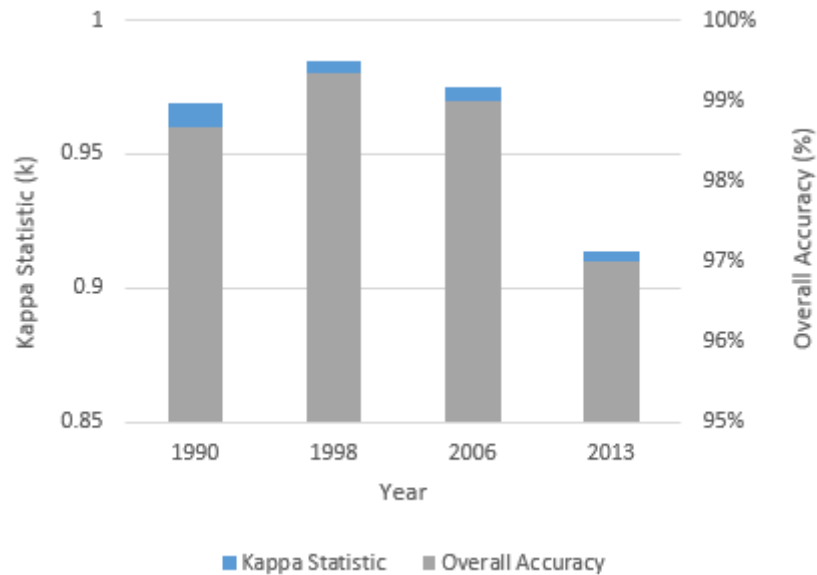
Figure 4.5: Overall accuracy (%) and Kappa Statistics (*k*) of 1990, 1998, 2006 and 2013 Landsat images.

Producer and User Accuracy statistics for each feature class is listed in Table 4.1 for the year 1990. The error matrix (Table 4.5) displays that 66 water pixels were correctly classified as *Water,* resulting in a User Accuracy of 100%. A single pixel from the *Other* classification was incorrectly classified as *Water,* resulting in a Producers Accuracy of 98.51%. Next, 215 *Other* pixels were correctly classified resulting in the Users Accuracy of 99.54%. A classification error in this category occurred where 3 *Vegetation* pixels were incorrectly classified as other pixels resulting in a Producers Accuracy of 98.62%. Both Producer and User Accuracies of *Saline Features* were classified without error. This is partly due to *Saline Features* being the smallest classified feature in the image and as such, this feature received very few random sampling points

during the accuracy assessment. *Vegetation* pixels were the most misclassified pixels of the 1990 image with a User's Accuracy of 80% and a moderate Kappa coefficient of 0.79. For 1990 (Figure 4.1), the classification accuracy of *Vegetation* pixels was the least reliable of all features.

Table 4.1: Accuracy statistics report (of 300 random sampling points) for Landsat 5 (1990) image aggregation from unsupervised ISODATA classification.

Class Name	Producer's Accuracy	95% Confidence Interval	User's Accuracy	95% Confidence Interval	Kappa Statistic
Water	98.507%	(94.858% 102.157%)	100.00%	(99.242% 100.758%)	1.0000
Other	98.624%	(96.848% 100.400%)	99.537%	(98.400% 100.674%)	0.9831
Vegetation	100.000%	(95.833% 104.167%)	80.000%	(56.424% 103.576%)	0.7917
Saline Features	100.000%	(83.333% 116.667%)	100.000%	(83.333% 116.667%)	1.0000
Overall Accuracy: 98.667%			**95% Confidence Interval (97.202% 100.131%)**		
Overall Kappa Statistic: 0.969			**Overall Kappa Variance: 0.000**		

Table 4.2: Error (Confusion) Matrix accuracy report (of 300 random sampling points) for Landsat 5 (1990) image aggregation from unsupervised ISODATA classification.

Classified Data			Reference Data		
	Water	*Other*	*Vegetation*	*Saline Features*	**Totals**
Water	66	0	0	0	66
Other	1	215	0	0	216
Vegetation	0	3	12	0	15
Saline Features	0	0	0	3	3
Totals	67	218	12	3	300

As displayed in Table 4.3, both the overall accuracy and Kappa statistics increased in the 1998 image (Figure 4.2) classification to 99.33% and 0.985 respectively. Problems of pixel classification accuracy significantly decreased in the 1998 image by only showing conflict between the *Water* and *Other* feature classes. Of 71 *Water* classified pixels in the image, 69 pixels were correctly classified resulting in a user accuracy of 97.18%. The other 2 pixels were mistakenly classified into the *Other* feature classification resulting in a producer's accuracy of 99.07 in the other feature class. The remaining pixels were classified 100% accurate against the reference image and do not display any risk for being classified by chance (as displayed in Table

4.4). Similar instances of error have occurred amongst the *Water* and *Other* feature classifications between 1990 and 1998. This can be identified from both the classified image, where the majority of the *Water* class borders onto *Other* features classification; as well in the reference image where the shoreline pixels are visibly the most complex pixels in the image for differentiating between two classifications.

Table 4.3: Accuracy statistics report (of 300 random sampling points) for Landsat 5 (1998) image aggregation from unsupervised ISODATA classification.

Class Name	Producer's Accuracy	95% Confidence Interval	User's Accuracy	95% Confidence Interval	Kappa Statistic
Water	100.000%	(99.275% 100.725%)	97.183%	(92.630% 101.736%)	0.9634
Other	99.065%	(97.543% 100.588%)	100.000%	(99.764% 100.236%)	1.0000
Vegetation	100.000%	(96.875% 103.125%)	100.000%	(96.875% 103.125%)	1.0000
Saline Features	100.000%	(50.000% 150.000%)	100.000%	(50.000% 150.000%)	1.0000
Overall Accuracy: 99.333%			**95% Confidence Interval (98.246% 100.421%)**		
Overall Kappa Statistic: 0.985			**Overall Kappa Variance: 0.000**		

Table 4.4: Error (Confusion) Matrix accuracy report (of 300 random sampling points) for Landsat 5 (1998) image aggregation from unsupervised ISODATA classification.

Classified Data	Reference Data				
	Water	*Other*	*Vegetation*	*Saline Features*	**Totals**
Water	69	2	0	0	71
Other	0	212	0	0	212
Vegetation	0	0	16	0	16
Saline Features	0	0	0	1	1
Totals	69	214	16	1	300

Table 4.5 shows the overall accuracy and Kappa statistics from the 2006 accuracy assessment begin to decline from 1998. The movement of accuracy statistics displayed in Figure 4.5 mirrors the decline of the lakes size itself. This may inform both the producer and the user of these image classifications that as the environment in question becomes increasingly complicated.

This can be attributed to environmental degradation where pixel classification can become increasing exposed to instances of omission and commission errors.

In the 2006 image classification (Figure 4.3) all but 1 *Water* pixel (Table 4.6) was omitted from the dataset and committed to another, resulting in both a producer and user accuracy of 98.077%. The same degree of error occurred when classifying *Other* pixels, resulting in user and producers accuracies of 99.558%. Of the images used in this analysis, 2006 is the first year where the Kappa coefficient of *Saline Features* classification has decreased from $k = 1$, yet at 0.83, it still maintains that pixel classification was unlikely due to chance (Lentilucci, 2006).

Table 4.5: Accuracy statistics report (of 300 random sampling points) for Landsat 5 (2006) image aggregation from unsupervised ISODATA classification.

Class Name	Producer's Accuracy	95% Confidence Interval	User's Accuracy	95% Confidence Interval	Kappa Statistic
Water	98.077%	(93.383% 102.771%)	98.077%	(93.383% 102.771%)	0.9767
Other	99.558%	(98.471% 100.644%)	99.558%	(98.471% 100.644%)	0.9821
Vegetation	100.000%	(96.875% 103.125%)	100.000%	(96.875% 103.125%)	1.0000
Saline Features	83.333%	(45.180% 121.487%)	83.333%	(45.180% 121.487%)	0.8299
Overall Accuracy: 99.000%			**95% Confidence Interval (97.707% 100.293%)**		
Overall Kappa Statistic: 0.975			**Overall Kappa Variance: 0.000**		

Table 4.6: Error (Confusion) Matrix accuracy report (of 300 random sampling points) for Landsat 5 (2006) image aggregation from unsupervised ISODATA classification.

Classified Data			Reference Data		
	Water	*Other*	*Vegetation*	*Saline Features*	**Totals**
Water	51	1	0	0	52
Other	0	225	0	1	226
Vegetation	0	0	16	0	16
Saline Features	1	0	0	5	6
Totals	52	226	16	6	300

The 2013 image classification (Figure 4.4) had the lowest accuracy statistics for the period of analysis. Overall accuracy of the image was reduced to 97% with a Kappa statistic of

0.914 (Table 4.7). The *Other* feature class showed the most instances of incorrectly classified pixels (Table 4.8). As well, the *Saline Features* class had the most errors against the reference image where only 71.4% of classified *Saline Features* pixels represent saline features in reality. The Kappa statistics for *Saline Features* pixel classification was reduced further from 2006 to $k = 0.7$, which shows increasing probabilities of pixels being classified as salinity merely by chance.

Table 4.7: Accuracy statistics report (of 300 random sampling points) for Landsat 8 (2013) image aggregation from unsupervised ISODATA classification.

Class Name	Producer's Accuracy	95% Confidence Interval	User's Accuracy	95% Confidence Interval	Kappa Statistic
Water	96.154%	(86.839% 105.469%)	96.154%	(86.839% 105.469%)	0.9579
Other	97.107%	(94.789% 99.426%)	99.576%	(98.536% 100.617%)	0.9781
Vegetation	95.455%	(84.478% 106.432%)	87.500%	(72.185% 102.815%)	0.8651
Saline Features	100.000%	(95.000% 105.000%)	71.429%	(44.193% 98.664%)	0.7044
Overall Accuracy: 97.000%			**95% Confidence Interval (94.903% 99.097%)**		
Overall Kappa Statistic: 0.914			**Overall Kappa Variance: 0.001**		

Table 4.8: Error (Confusion) Matrix accuracy report (of 300 random sampling points) for Landsat 8 (2013) image aggregation from unsupervised ISODATA classification.

Classified Data	Reference Data				
	Water	*Other*	*Vegetation*	*Saline Features*	**Totals**
Water	25	1	0	0	26
Other	1	235	0	0	236
Vegetation	0	3	21	0	24
Saline Features	0	3	1	10	14
Totals	26	242	22	10	300

In general, the overall accuracy statistics from 1990, 1998, 2006 and 2013 image classifications are acceptable. It is important to note however, that overall accuracies are not capable of giving insight into individual classification errors. By analyzing individual feature class changes, one can explain changes in overall accuracy. For instance, the *Saline Features* classification becomes more unreliable as a realistic measure of pixel representation from 1990 to 2013. As well, when visually assessing change over time from the image classification output

29

maps themselves, errors of omission and commission highlight faults of the producers, and faults within the classification process. To use the *Saline Features* pixel classifications as another example, the trend of its accuracy statistics over time speaks to the unpredictable and random nature of salinity and saline features, especially loose evaporites. In contrast, water bodies as a main image feature will generally be less difficult to accurately classify as *Water* based on its size, consistency over space, and unmistakable absorption characteristics. Relative to the accuracy assessment process, large water bodies such as Lake Urmia can be unmistakable when classifying a random sampling point against the reference image. Shorelines can create classification discrepancies in the random sampling process when image resolution and lack of additional data hinder classification accuracy of complex shorelines.

4.3 Band Differencing

As stated earlier in the methods section, the NIR band was selected for the band differencing analysis for its strengths in differentiating between land type boundaries. A value of 0 in a band differencing image represents no change in reflectance values of a pixel between two time periods (Cho and Ntoulas, 2002). Thresholds of standard deviation were applied to better identify greater extremes of change, while also grouping together pixels showing limited change (above or below 0). Descriptive statistics from each band differencing image are listed in Table 4.9 to show how values in output images were classified and interpreted for degrees of change.

Table 4.9: Descriptive statistics of NIR band differencing image values.

Image Statistics	1990-1998	1998-2006	2006-2013*
Minimum	-173	-185	6169
Maximum	182	177	38339
Mean	-32	12	18996
Standard Deviation	82	95	7322
½ Standard Deviation	41	~48	3661
*2006-2013 band differencing image conducted on non-TOA corrected NIR band due to software limitations			

All images were classified with one half standard deviation thresholds, snapped to their minimum and maximum values when required. The first time period was analyzed using the near infrared band by subtracting the NIR band 4 in the 1990 image from the 1998 image using raster calculator in ArcGIS (Figure 4.6). Values between -31.99 and 9 were identified as the threshold of no change between 1990 and 1998. Change values in the 1998 to 2006 image (Figure 4.7) were identified by one half standard deviations from the mean, just as for the 1990 to 1998 image. The values ranging from -35.99 to 12 represent the threshold of no change pixels between 2006 and 1998. Lastly, the band differencing image from 2006 to 2013 (Figure 4.8) poses its own challenge. Being limited to PCI Geomatica 2013 (which does not include algorithm options for Landsat 8 imagery), the NIR bands from 2006 and 2013 used for this band differencing analysis were not TOA corrected (Table 4.9). Therefore the output values from the raster calculation represent DN values instead of reflectance values. However, it was still possible to classify the change values by one half standard deviation to identify the threshold for no change. In this case, all values below the mean were labelled as pixels representing no change in the band differencing output image between 2006 and 2013.

Between 1990 and 1998 Lake Urmia increased in size, most noticeably along the northeast shoreline. There was also an increase in *Saline Features* during this period.. From 1998 to 2006 there is a significant amount of water loss in the image, most noticeably at the northeast and southeast extents of the lake. Increasing reflectiveness in pixels corresponds to evaporation of highly absorptive *Water* pixels, and newly exposed salt-laden lakebed. Pixels representing feature loss are scattered throughout the surrounding environment that may be indicative of drought impacts on vegetation. Lastly, there are no instances of decreased pixel reflectance in the output image from 2006 and 2013.
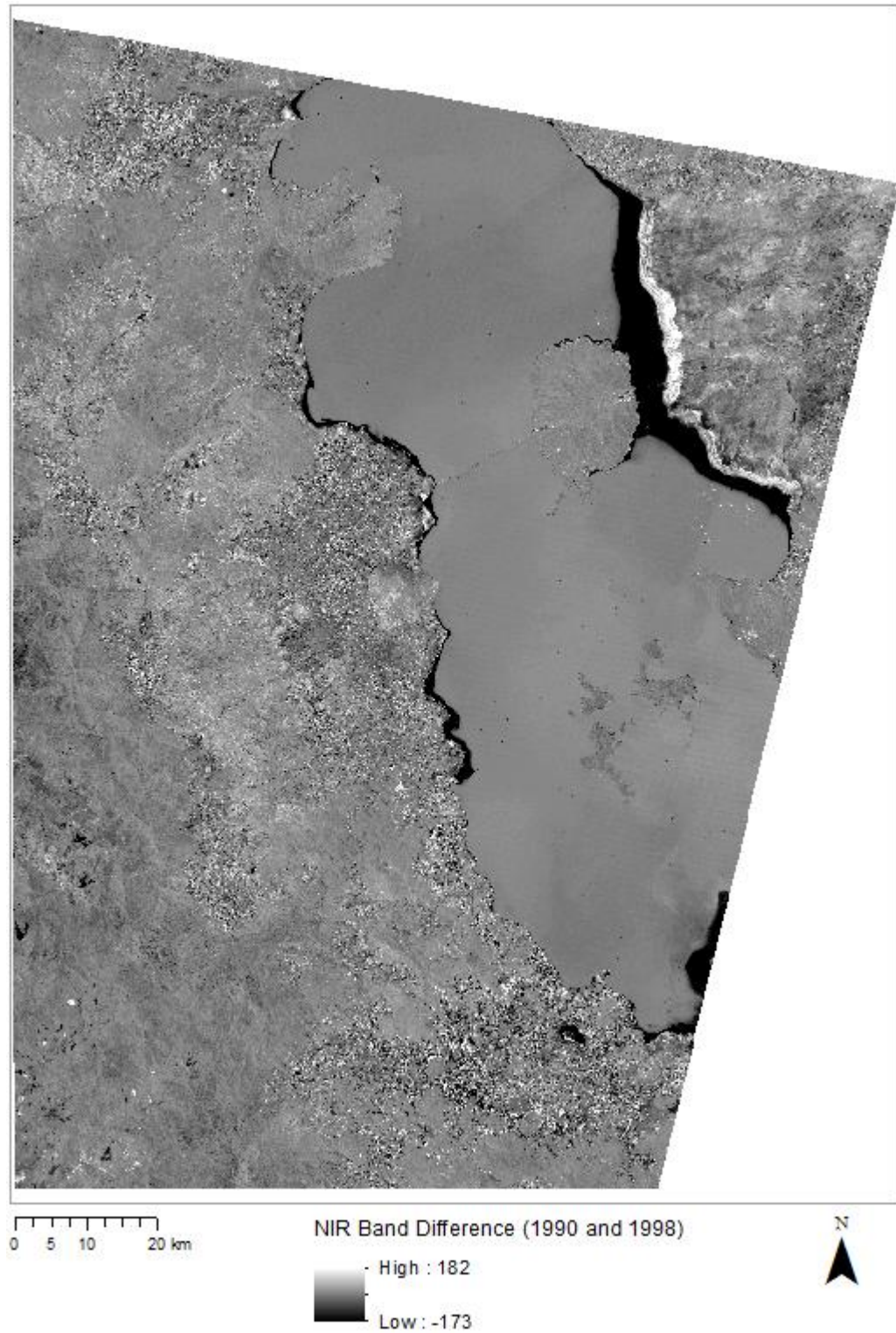
Figure 4.6: NIR band differencing image 1990 and 1998. Where white – positive (high) change, black – negative (low) change, grey – no change.
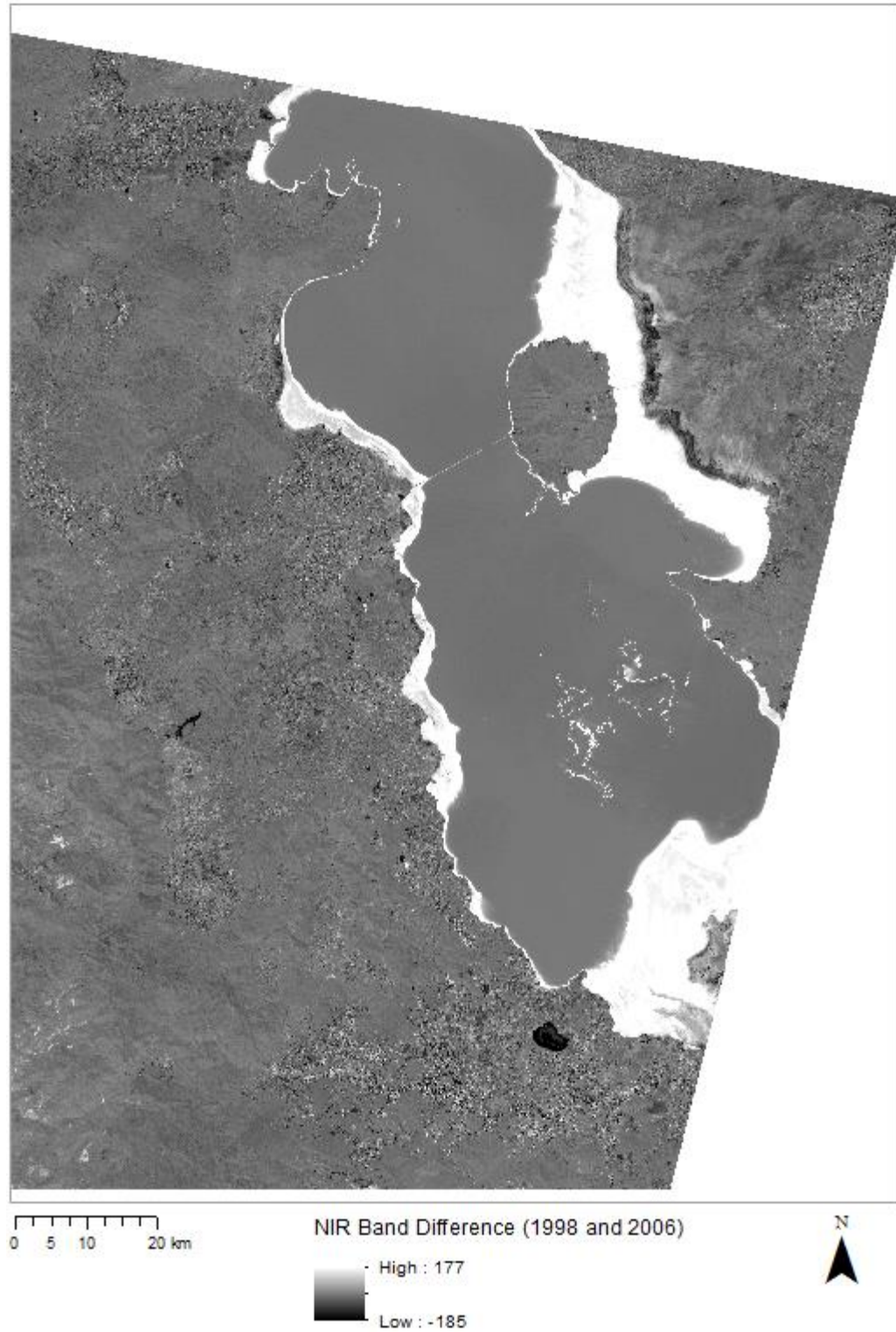
Figure 4.7: NIR band differencing image 1998 and 2006. Where white – positive (high) change, black – negative (low) change, grey – no change.
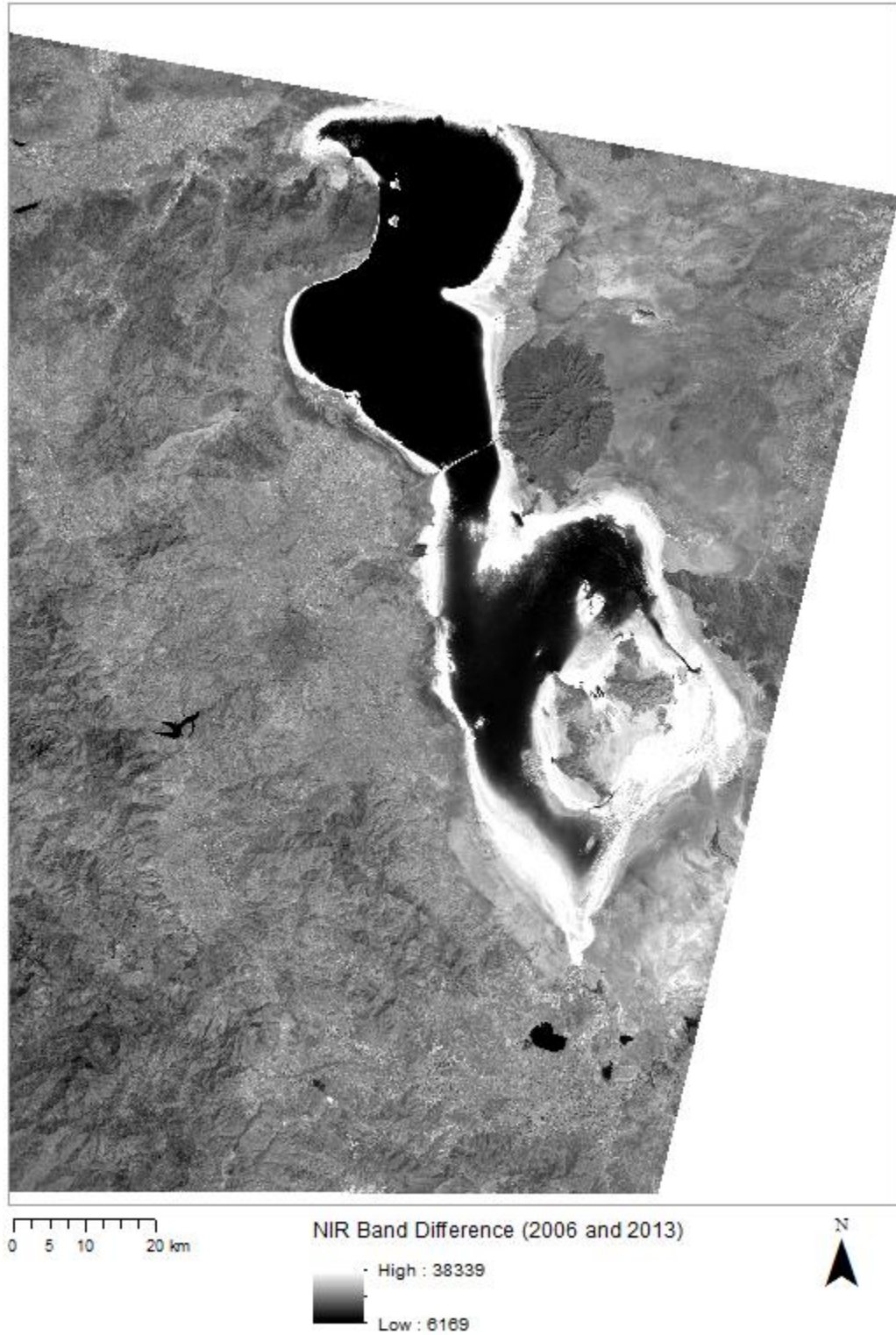
Figure 4.8: NIR band differencing image 2006 and 2013. Where white – positive (high) change, black – negative (low) change, grey – no change.

4.4 Change Detection, 1990 and 1998

Natural fluctuations of water levels at Lake Urmia were reported by Pengra (2012), Zarrineh and Azari Najaf Abad (2014) up until 1998. The causeway was in early stages of construction during this point in the analysis (Khalyani *et al.,* 2014), and did not appear to have any impact on the lake between 1990 and 1998.

Class 201 – "Growth of *Water*" shows the increasing lake size in Figure 4.9. Pixels identifying water appear clustered as a homogenous feature class. Pixels labelled as 304 – "Growth of *Saline Features*" outlines the increased presence of salinity between the two years. Pixels identifying salinity display the scattered characteristics of salinization. Additionally, the *Saline Features* identified in Figure 4.9 should represent relatively recent processes of salinization based on their reflectiveness. As Csillag *et al.* (1993), Farifteh *et al.* (2006) and Allbed and Kumar (2013) identified in soil salinity studies, reflectiveness of salt diminishes as evaporites become mixed with other soils and pollutants. A scattering of pixels labelled as 303 – "Growth of *Vegetation*" highlight increased reflectance of vegetation pixels. An increase in reflectiveness of vegetation pixels in the NIR band can be interpreted as growth of healthy crops between 1990 and 1998. Vegetative growth and increased lake size mirror the lessened rate of evaporation at Lake Urmia between 1990 and 1998 (Faramarzi, 2012).

4.5 Change Detection, 1998 and 2006

During this time, the pipeline to Tabriz had opened and construction on the causeway was nearing completion (Khalyani *et al.,* 2014). By 2006, approximately 21 billion m³ of water would have been extracted from the Lake Urmia watershed, accounting for approximately 7.6 km² of surface water loss during this time. As the lake size decreased between 1998 and 2006, the contrasting lakebed emerged in its place, as identified by the yellow pixels (302 – "Growth of *Other*") surrounding the entire lake (Figure 4.10).

Figure 4.9: 1990 and 1998 Landsat 5 NIR band differencing image. Change detection atop background imagery of 1990 NIR band. Blue – Growth of *Water,* red – Growth of *Saline Features* and green – Growth of *Vegetation*.
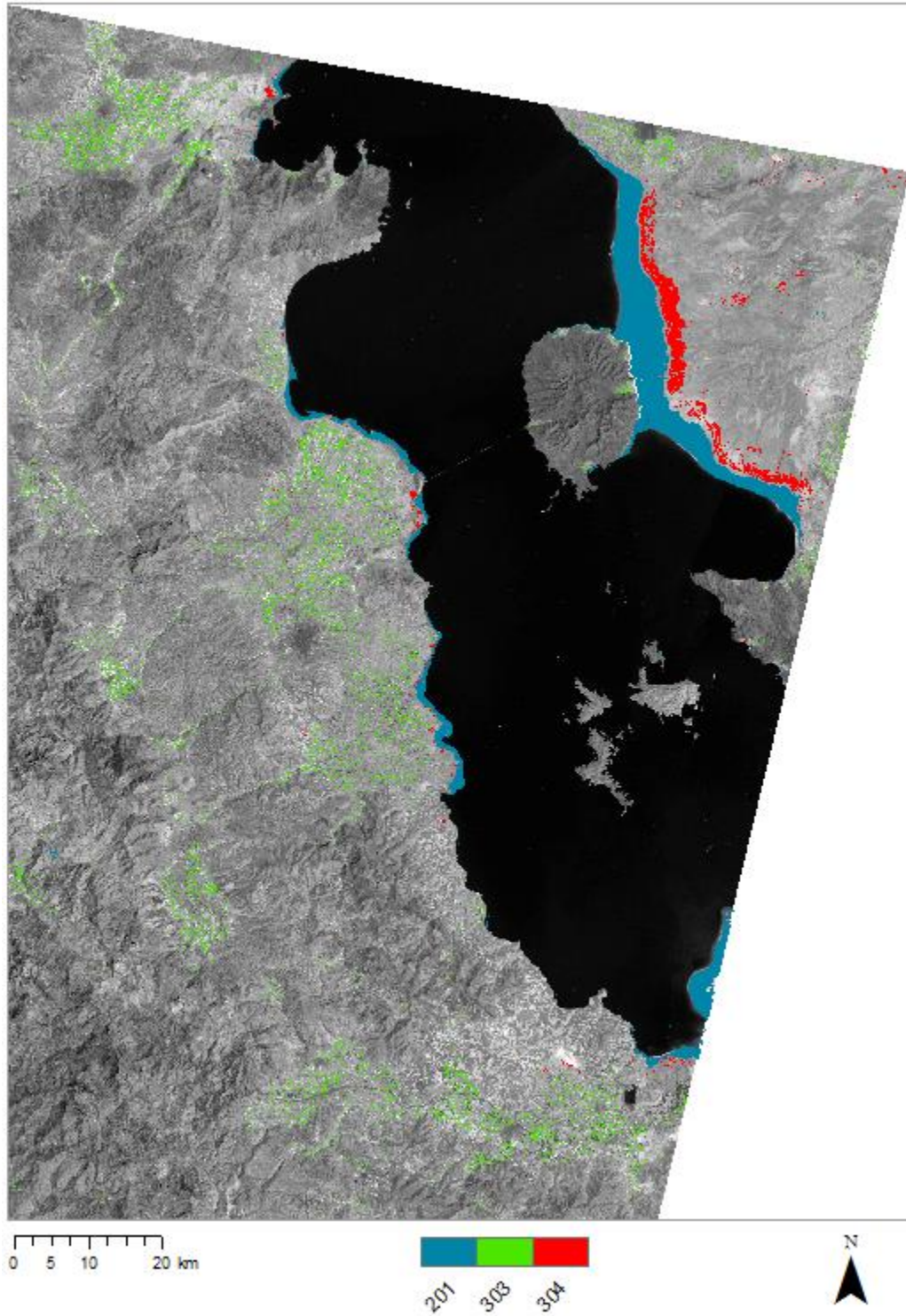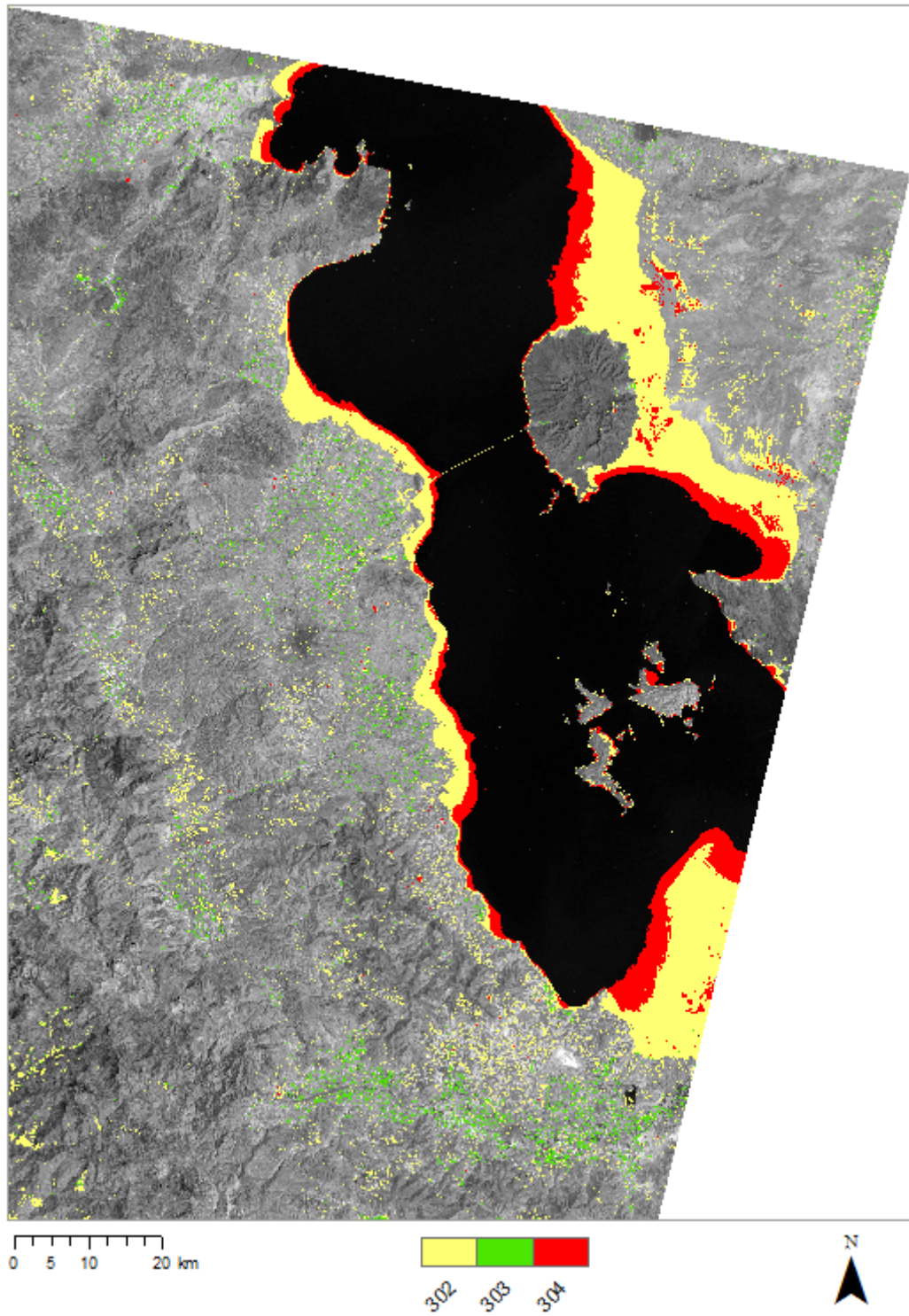
Figure 4.10: 1998 and 2006 Landsat 5 NIR band differencing image. Change detection atop background imagery of 1990 NIR band. Red – Growth of *Saline Features,* green – Growth of *Vegetation*, and yellow – Growth of *Other*.

Additional growth of saline features (304 – "Growth of *Saline Features*") is noticeable along the lakes shoreline, around mountains and along the causeway. Khalyani *et al.* (2014), Zarrineh and Azari Najaf Abad (2014) both suggest the demise of Lake Urmia was caused by the pipeline and causeway. The solid bridge structure began to influence the location of water loss and salinization between 1998 and 2006 as seen at the west entrance of the causeway.

4.6 Change Detection, 2006 and 2013

To accentuate temporal feature change from 2006 to 2013, the change detection output classes were overlaid atop the NIR band from 1990. The extent of Lake Urmia in 1990 (black) is contrasted with the extent of the lake in 2013 (class 101 – "No Change, *Water*"). Feature change became more complex throughout the lake, reflecting severe water loss and salinization. Where saline features are no longer identified in previous images, it is likely that the saline evaporite particles have been blown elsewhere by frequent windstorms throughout the region (Grotzinger *et al.,* 2007). As mentioned previously, there are varying depths of water throughout the remainder of the lake, which was not the case in previous images. Class 301, interpreted as "Loss of *Water*" identifies pixels representing water that have become more reflective over time. By referring to the 2013 natural colour image, it was determined that this classification was detecting areas within the lake that have become shallower. The southern portion of the lake is significantly less saline than the north, allowing for faster rates of evaporation than highly saline water (Karbassi *et al.*, 2010). Future predictions of water volume loss in the lake can be made from the unequal lake depths and saline concentrations.

If the pipeline continued to extract water from the watershed at the rate of 3 billion m³ per year (Khalyani *et al.,* 2014), by 2013 42 billion m³ of water could have been withdrawn since 1999, accounting for approximately 12 km² of surface water loss during this time. Additionally, the completion of the causeway in 2008 appears to exacerbate the process of salinization along the length of the bridge (highlighted by class 304 – "Growth of *Saline Features*"). The lakebed

will be continuously exposed (represented as 302 – "Growth of *Other*") as the surface water continues to shrink in size. Reflectiveness of vegetation appears to be present and growing up to 2013, which can be linked to increasing resource demands and resource extraction from Lake Urmia.

Logical inferences about feature changes between 1990 and 2013 can be made from Figure 4.11. Pixels representing water have likely changed to represent saline features and the exposed lakebed. Some saline features have remained at the same location over this analysis. However, it can be predicted that due to the transitory nature of saline evaporites, the location of *Saline Features* in 2013 will change in years to come.

4.7 Overall Lake Change

The maximum (1998) and minimum (2013) extents of Lake Urmia during this analysis are visualized in Figure 4.12. From the classified images, the lake surface area measured 4995 km² in 1998 and 1849 km² in 2013. During this time period, three events contributed to the diminishing size of the lake: construction of the Tabriz pipeline in 1999 (Khalyani *et al.,* 2014), completion of the Urmia causeway in 2008 (Kabiri *et al.,* 2012) and excessively dry climatic conditions (World Bank, 2014). Zeinoddini *et al.* (2014) reported the yearly rate of evaporation at Lake Urmia to be 1020mm/year (85mm/month). In contrast to the yearly average precipitation of 264 mm/year (22mm/month) recorded by the World Bank (2014), it is clear that this region is suffering from a water deficit.
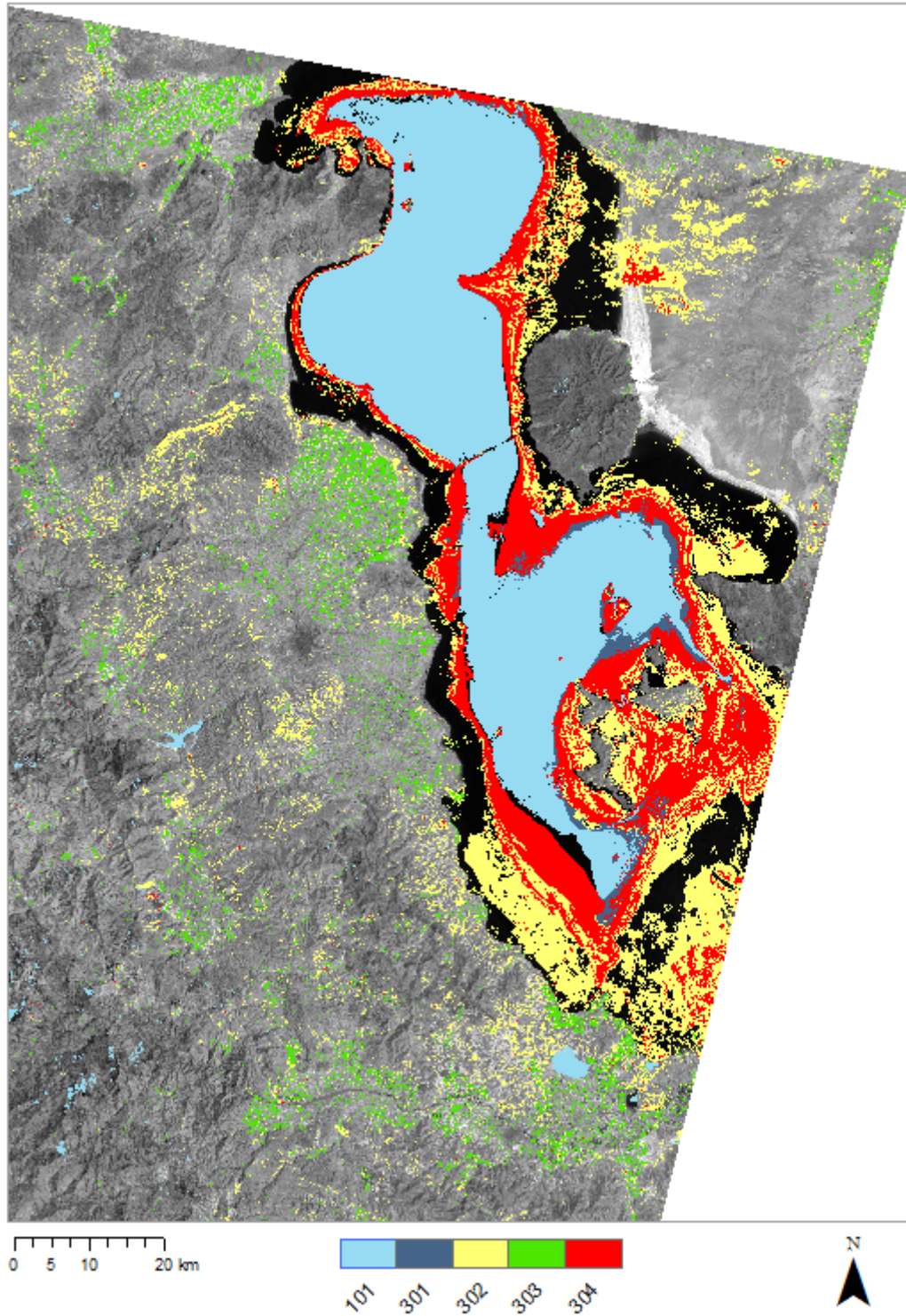
Figure 4.11: 2006 Landsat 5 and 2013 Landsat 8 NIR band differencing image. Change atop background imagery of 1990 NIR band (black outlines the lake extent in 1990). Light blue – No Change *Water*, blue – Loss of *Water*, red – Growth of *Saline Features*, green – Growth of *Vegetation* and yellow – Growth of *Other*.

Figure 4.12: Change in lake size. From maximum extent of 4995 km² (1998 – dark blue) to minimum extent of 1849 km² (2013 – light blue) during the period of analysis.

CHAPTER FIVE: Conclusion

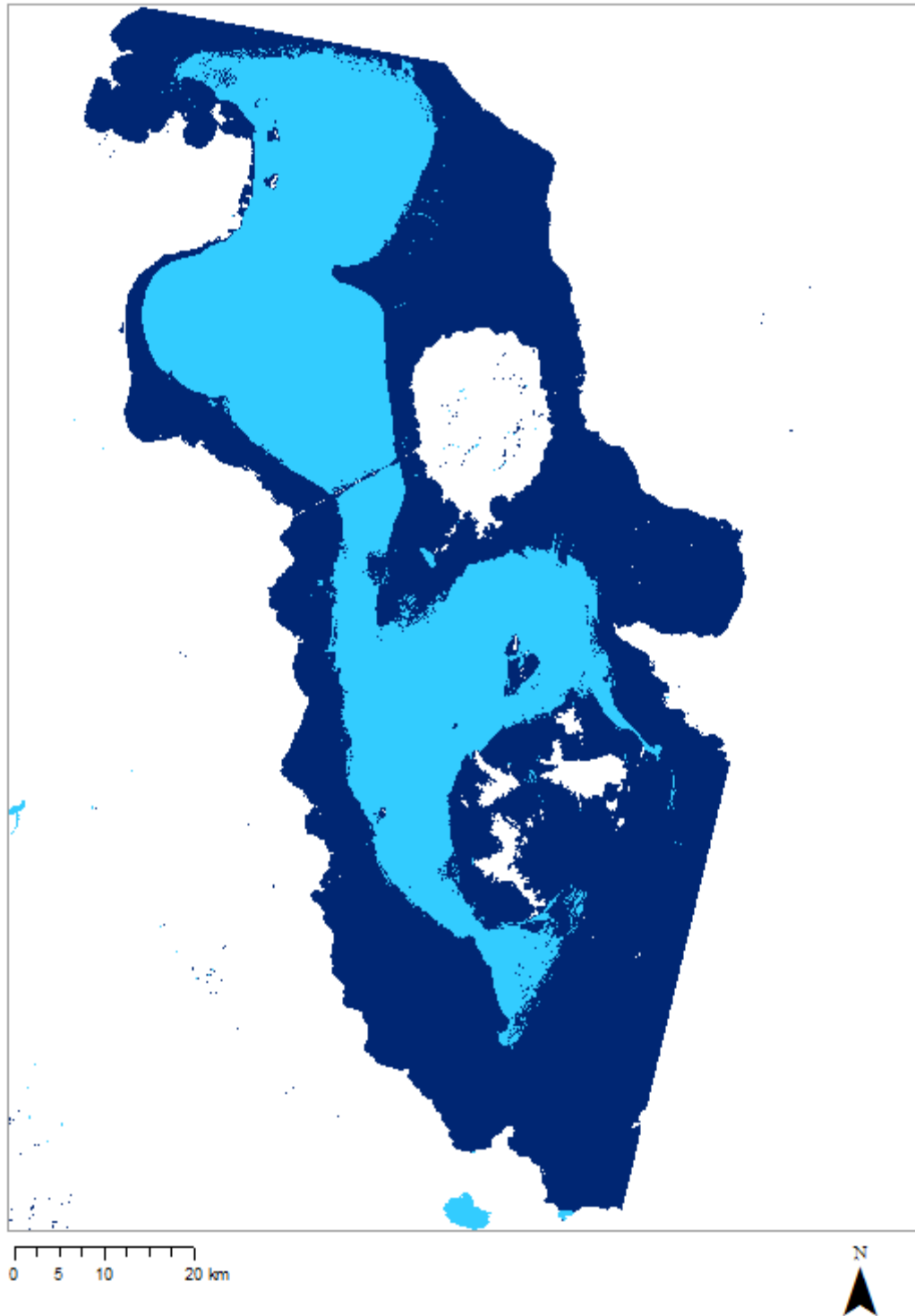The classification framework and change detection analysis in this study provided two conclusions. Firstly, this remote sensing based study of salinization at Lake Urmia successfully produced visual representations of feature changes between 1990, 1998, 2006 and 2013.

Multispectral imagery was successful in conducting a land cover change detection analysis. The data fit the scope of the study and were easily accessible. However, higher spatial resolution in some bands of the Landsat 8 image made for easier feature delineation and identification than the Landsat 5 imagery. Confidence in the classification methods is attributed to consistently high (>90%) overall accuracy statistics derived from the post-classification analysis.

Secondly, the change detection analysis of land cover from 1990 to 2013 highlights the growth of salinized land aggressively overtaking Lake Urmia and its immediate environment. The dry region has most certainly become drier since 1998 from both climatic and anthropogenic stresses. This can be seen in the change detection maps where "Growth of *Other*" (302 – yellow) and "Growth of *Saline Features*" (304 – red) classes are the most prominent in 2013. Together these classes highlight the expanding drought-like conditions throughout the environment.

Water resource extraction for market crop agriculture and urban development is not a suitable long-term strategy for economic prosperity. Water-intensive practices were not meant to be sustainable in arid climates, meaning Lake Urmia has always been vulnerable to changes in its water cycle. Looking to the future, Iranians must be willing to adapt to a life without Lake Urmia, or begin to make every attempt to nurse the lake back to a healthy state.

5.1 Limitations

As the environment so drastically changed between years of analysis, 30m resolution imagery should be accompanied with additional data to better illustrate complex boundaries and features. Google usually provides a wealth of open source geospatial data, yet neither Google

Earth nor Google Street View has mapped Iran in its usual fashion (for privacy and political concerns). It was nearly impossible to acquire any additional imagery, photographs or data.

5.2 Contribution to Research and Implications

The best band combinations for identifying Lake Urmia and salinization included the blue, near infrared, thermal infrared and Tasselled Cap Transformation brightness and wetness bands. As the literature suggests (Verma *et al.,* 1994; Goossens *et al.,* 1999; Howari, 2002; Allbed and Kumar, 2013) the use of the thermal infrared band enhanced identification of *Saline Features*. In addition, the brightness and wetness bands of the TCT accentuated salinity, and land-water boundaries. It was therefore beneficial to the image classification process and output to call attention to boundary differentiation of land cover types and their measures of brightness. The NIR, TIR and TCT bands were recommended in numerous remote sensing based studies of salinization (Verma *et al.,* 1994; Peng, 1998; Metternick and Zinck, 2003; Masoud and Koike, 2006; Elnagger and Noller, 2009). In combination, these bands proved to successfully identify saline features from multispectral images.

Public demonstrations for the protection and revitalization of Lake Urmia would benefit from the output maps of this change detection analysis. Used as visual evidence of water loss and salinization, the general public would be equipped with factual representations of recent environmental changes.

5.3 Future Research

This study focused its efforts to identifying water loss and the salinization of land cover with minimal inferences to effects of salinity on vegetation (secondary indicators). By continuing to identify and monitor land cover change over time, studies driven by vegetation analysis would add another dimension to salinity-based studies of Lake Urmia and its region.

REFERENCES

Abbaspour, M., A.H. Javod, S.A. Mirbagheri, F. Ahmadi Givi, and P. Moghimi. 2012. Investigation of Lake Drying Attributed to Climate Change. *International Journal of Environmental Science and Technology.* Vol. 9, No. 2, pp. 257-266.

Allbed, A., and L. Kumar. 2013. Soil Salinity Mapping and Monitoring in Arid and Semi-Arid Regions Using Remote Sensing Technology: A Review. *Advances in Remote Sensing.* Vol. 2, No. 4. pp. 373-385.

ArcGIS Help 10.1. 2014. Tasseled Cap Transformations. *ArcGIS Resources.* May 18, 2014. Available Online: http://resources.arcgis.com/en/help/main/10.1/index.html#//009t0000024t000000

Ayboga, E., and A. Ilhan. 2012. Iran's Dam Policy and the Case of the Lake Urmia. *Ekopotamya.* July 12, 2012. Available online: http://ekopotamya.net/index.php/2012/07/irans-dam-policy-and-the-case-of-the-lake-urmia/

Chang, C-T., J.Z.C. Lai and M-D. Jeng. 2011. A Fuzzy K-Means Clustering Algorithm Using Cluster Center Displacement. *Journal of Information Science and Engineering.* Vol. 27, pp. 995-1009.

Cho, J., and A. Ntoulas. 2002. Effective Change Detection Using Sampling. *Proceedings of the 28th VLDB Conference.* Hong-Kong, China. August 20-23, 2002.

Christopherson, R., and M.L. Bryne. 2009. Canadian Geosystems (Second Edition). Pearson Prentice Hall. Toronto, Ontario. 709pp.

Congalton, R.G. 1991. A Review of Assessing the Accuracy of Classifications of Remotely Sensed Data. *Remote Sensing of Environment.* Vol. 37, No. 1, pp. 35-46.

Crist, E.P., and R.C. Cicone. 1984. A Physically-Based Transformation of Thematic Mapper Data – The TM Tasseled Cap. *IEEE Transactions on Geoscience and Remote Sensing.* Vol. 22, No. 3, pp. 256-263.

Crowley, J.K. 1991. Visible and Near-Infrared (0.4-2.5/am) Reflectance Spectra of Playa Evaporite Minerals. *Journal of Geophysical Research.* Vol. 96, No. B10, pp. 231-240.

Csillag, F., L. Pasztore, and L.L. Biehl. 1993. Spectral Selection for Characterization of Salinity Status of Soils. *Remote Sensing of Environment.* Vol. 43, pp. 231-242.

Dehaan, R., and G.R. Taylor. 2003. Image-Derived Spectral Endmembers as Indicators of Salinization. *International Journal of Remote Sensing.* Vol. 24, No. 4. pp. 775-794.

Dehni, A., and M. Lounis. 2012. Remote Sensing Techniques for Salt Affected Soil Mapping: Application to the Oran Region of Algeria. *Procedia Engineering.* Vol. 33, pp. 188-198.

DeLorme. 2012. ArcGIS online: World Reference Overlay. Redlands, CA. Available online: http://www.arcgis.com/home/item.html?id=9763d83ba63048da8a2e0a71ccea4416

Driessen, P. M., and R. Schoorl. 1973. Mineralogy and Morphology of Salt Efflorescence on Saline Soils in the Great Konya Basin, Turkey. *Journal of Soil Science*. Vol. 24, No. 4 pp. 436– 442.

Dwivedi, R.S., K. Sreenivas, and K.V. Ramana. 1999. Inventory of Salt-Affected Soils and Waterlogged Areas: A Remote Sensing Approach. *International Journal of Remote Sensing*. Vol. 20, No. 8, pp. 1589-1599.

Eghbalm, M. K., J. Southard, and L.D. Whittig. 1989. Dynamics of Evaporite Distribution in Soils on a Fan– Playa Transect in the Carrizo Plain California. *Soil Science Society of America Journal*. Vol. 53, No. 3, pp. 898– 903.

Eimanifar, A., and F. Mohebbi. 2007. Urmia Lake (Northwest Iran): A Brief Review. *Saline Systems*. Vol. 3, No. 5, pp. 1-8.

Eklund, P.W., S.D. Kirkby, and A. Samlim. 1998. Data Mining and Soil Salinity Analysis. *International Journal of Geographic Information Science.* Vol. 12, No. 3, pp. 247– 268.

Elnaggar, A.A., and J. S. Noller. 2009. Application of Remote- Sensing Data and Decision-Tree Analysis to Mapping Salt- Affected Soils over Large Areas. *Remote Sensing*. Vol. 2, No. 1, pp. 151-165.

Esri. 2012. ArcGIS online: World Reference Overlay. Redlands, CA.
Available online:
http://www.arcgis.com/home/item.html?id=9763d83ba63048da8a2e0a71ccea4416

Faramarzi, N. 2012. Agricultural Water Use in Lake Urmia Basin, Iran: An Approach to Adaptive Policies and Transition to Sustainable Irrigation Water Use. Department of Earth Sciences. Uppsala University. 44pp.

Farifteh, J., A. Farshad, and R.J. George. 2006. Assessing Salt-Affected Soils Using Remote Sensing, Solute Modelling, and Geophysics. *Geoderma.* Vol. 130, No. 3-4. pp. 191-206.

Fernandez-Buces, N., C. Siebe, S. Cram and J. L. Palacio. 2006. Mapping Soil Salinity Using a Combined Spectral Response Index for Bare Soil and Vegetation: A Case Study in the Former Lake Texcoco, Mexico. *Journal of Arid Environments*. Vol. 65, No. 4, pp. 644-667.

Forsythe, K.W., and G. McCartney. 2014. Investigating Forest Disturbance Using Landsat Data in the Nagagamisis Central Plateau, Ontario, Canada. *International Journal of Geo-Information.* Vol. 3, No. 1, pp. 254-273.

Garousi, V., A. Najafi, A. Samadi, K. Rasouli, and B. Khanaliloo. 2013. Environmental Crisis in Lake Urmia, Iran: A Systematic Review of Causes, Negative Consequences and Possible Solutions. *Lake Urmia Conservation Institute.* January 2013. Available online: http://people.ucalgary.ca/~vgarousi/downloads/papers/conf/2013_IPWE/IPWE%202013_Lake%20Urmia_SLR.pdf

Google Earth Version 71.2.2014. 2013. East Azerbaijan, Iran. 37° 44' 22.96"N, 45° 41' 02.87"E. Basarsoft, U.S. Department of State Geography. Available online: earth.google.com

Goossens, R., A. P. S. Kazem, M. De Dapper and O. Kis-syar. 1999. The Use of Thermal Band of Landsat TM for the Study of Soil Salinity in Iran (Ardakan Area) and Egypt (Ismailia Province). *Proceedings of the International conference on Geoinformatics for Natural Resource Assessment, Monitoring and Management.* Dehradun, India. March 3-11, 1999.

Grotzinger, J., T.H. Jordan, F. Press, and R. Siever. 2007. Understanding Earth (Fifth Edition). W.H. Freeman and Company, New York, USA. 579pp.

Howari, F. 2002. Spectroscopy of Evaporites. *Periodico di Mineralogia.* Vol. 71, No. 2. pp. 191-200.

Hunt, G., J. Salisbury, and C. Lenhoff. 1972. Visible and Near Infrared Spectra of Minerals and Rocks: V. Halides, Phosphates, Arsenates, Venadates and Borates. *Modern Geology.* Vol. 3, pp. 121– 132.

Kabiri, K., B. Pradhan, A. Sharifi, Y. Ghobadi, and S. Pirasteh. 2012. Manifestation of Remotely Sensed Data Coupled With Field Measured Meteorological Data for an Assessment of Degradation of Urmia Lake, Iran. *Proceedings of the Asia Pacific Conference on Environmental Science and Technology.* Kuala Lumpur, Malaysia. February 1-2, 2012.

Karbassi, A., G.N. Bidhendi, A. Pejman, and M.E. Bidhendi. 2010. Environmental Impacts of Desalinization on Ecology of Lake Urmia. *Journal of Great Lakes Research.* Vol. 36, No. 3, pp. 419-424.

Kauth, R.J. and G.S. Thomas. 1976. The Tasselled Cap -- A Graphic Description of the Spectral-Temporal Development of Agricultural Crops as Seen by LANDSAT. *Proceedings of the Symposium on Machine Processing of Remotely Sense Data.* IEEE Catalogue Number 76CH11031.

Khalyani, A.H., A.L. Mayer and E.S. Norman. 2014. Water Flows Towards Power: Socioecological Degradation of Lake Urmia, Iran. *Society and Natural Resources: An International Journal.* Vol. 27, No. 7, pp. 759-767.

Koshal, A.K. 2012. Spectral Characteristics of Soil Salinity Areas in Parts of South-West Punjab through Remote Sensing and GIS. *International Journal of Remote Sensing and GIS.* Vol. 1, No. 2, pp. 84-89.

Lentilucci, E.J. 2006. On Using and Computing the Kappa Statistic. Center for Imaging Sciences (CIS). Rochester Institute of Technology. 7pp.

Masoud, A.A. and K. Koike. 2006. Arid Land Salinization Detected by Remotely-Sensed Landcover Changes: A Case Study in the Siwa Region, NW Egypt. *Journal of Arid Environments.* Vol. 66, No. 1, pp. 151-167.

McMullen, B. 2000. SOILpak for Vegetable Growers. New South Wales (NSW) Agriculture. Warriewood, NSW.

Memarsadeghi, N., D.M. Mount, N.S. Netanyahu, and J. Le Moigne. 2006. A Fast Implementation of the ISODATA Clustering Algorithm. *International Journal of Computational Geometry and Applications.* Vol. 17, No. 1, pp. 71-103.

Metternicht, G.I., and J.A. Zinck. 2003. Remote Sensing of Soil Salinity: Potentials and Constraints. *Remote Sensing of Environment.* Vol. 85, No. 1, pp. 1-20.

Metternicht, G.I. and J.A. Zinck. 2010. Spatial Discrimination of Salt and Sodium-Affected Soil Surfaces. *International Journal of Remote Sensing*. Vol. 18, No. 12, pp. 2571-2586.

Mougenot, B., G.F. Epema, and M. Pouget. 1993. Remote Sensing of Salt Affected Soils. *Remote Sensing Review.* Vol. 7, No. 3-4, pp. 241-259.

Mulder, V.L., S. de Bruin, M.E. Schaepman, and T.R. Mayr. 2011. The Use of Remote Sensing in Soil and Terrain Mapping — a Review. *Geoderma.* Vol. 162, No. 1-2, pp. 1-19.

Naseri, M. Y. 1998. Characterization of Salt-Affected Soils for Modelling Sustainable Land Management in Semi-Arid Environment: a Case Study in the Gorgan region, Northeast Iran. ITC Publication. Australia. 321pp.

National Park Service (NPS). 2012. ArcGIS online: World Reference Overlay. Redlands, CA. Available online: http://www.arcgis.com/home/item.html?id=9763d83ba63048da8a2e0a71ccea4416

Noroozi, E. 2014. Saving Dying Lake is Priority for Iranian Leader [Photograph]. February 16, 2014. Available online: http://roxanasaberi.com/category/uncategorized/page/3

PCI Inc. 2010. PCI Help Menu. Richmond Hill, Ontario, Canada

Peng, W. 1998. Synthetic Analysis for Extracting Information on Soil Salinity Using Remote Sensing and GIS: A Case Study of Yanggao Basin in China. *Environmental Management.* Vol. 22, No. 1, pp. 153-159.

Pengra, B. 2012. The Drying of Iran's Lake Urmia and its Environmental Consequences. *UNEP Global Environmental Alert Services.* February 2012. Available online: http://www.unep.org/pdf/GEAS_Feb2012.pdf

Podmore, C. 2009. Dryland Salinity – Causes and Impacts. *Primefacts.* October, 2009. Available online: http://www.dpi.nsw.gov.au/__data/assets/pdf_file/0006/309381/Dryland-salinity-causes-and-impacts.pdf

Quinn, J.W. 2001. *Michael Emch Index.* April 9, 2002. Available online: http://web.pdx.edu/~emch/ip1/bandcombinations.html

Ramsar. 2010. Integrated Management Plan for Lake Urmia Basin. *The Ramsar Convention on Wetlands*. Available online: http://www.ramsar.org/pdf/wurc/LakeUrmiaManagementPlan-I.R.Iran2010.pdf

Sah, A.k., A. Eiumnoh, S. Murai, and P. Parkpian. 1995. Mapping of Salt-Affected Soils Using Remote Sensing and Geographic Information Systems: a Case Study of Nakhon Ratchaslma, Thailand. *Proceedings of the 16th Asian Conference Remote Sensing.* Nakhon Ratchasima, Thailand. November 20–24, 1995.

Schmid, T., M. Koch and J. Gumuzzio. 2008. Application of Hyperspectral Imagery to Soil

Salinity Mapping, In: G. Metternicht and J. Zinck, Eds., <u>Remote Sensing of Soil Salinization: Impact on Land Management</u>. CRC Press. Boca Raton, Florida. 377pp.

Scott, J.W., L.R. Moore, W.H. Harris, and M.D. Reed. 2003. Using the Landsat 7 Enhanced Thematic Mapper Tasseled Cap Transformation to Extract Shoreline. *U.S. Geological Survey Open-File Report of 03-272*. March, 2003. Available online: http://pubs.usgs.gov/of/2003/0272/OFR03-272.pdf

Setia, R., M. Lewis, P. Marschner, R. Raja Segaran, D. Summers, and D. Chittleborough. 2011. Severity of Salinity Accurately Detected and Classified on a Paddock Scale with High Resolution Multispectral Satellite Imagery. *Land Degradation and Development*. Vol. 24, No. 4, pp. 375-384.

Siegal, B. S., and A.R. Gillespie. 1980. <u>Remote Sensing in Geology</u>. Wiley. New York. 702pp.

Singh, R.P., and A. Sirohi, 1994. Spectral Reflectance Properties of Different Types of Soil Surfaces. *ISPRS Journal of Photogrammetry and Remote Sensing*. Vol. 49, No. 4, pp. 34-40.

Srestha, D.P**.** and A. Farshad. 2009. Mapping Salinity Hazard: an Integration Application of Remote Sensing and Modeling Based Techniques. In Zinck, A.J. and G. Mtternich. 2009. <u>Remote Sensing of Soil Salinization: Impact on Land Management.</u> CRC Press. Boca Raton. pp. 257-272.

Teggi, S., S. Costanzini, F. Despini, P. Chiodi, and F. Immordino. 2012. SPOT 5 Imagery for Soil Salinity Assessment in Iraq. *Proceedings of SPIE—Earth Resources and Environmental Remote Sensing/GIS Applications III*. Edinburgh, United Kingdom. September 24-27, 2012.

Urmulu, U. 2011. Lake Urmia Ecological Disaster [Photograph]. April, 2011. Available online: http://lake-urmia.blogspot.ca/2011/04/urmiye-golunun-quruams-ekoloji.html

U.S. Geological Survey. 2012.ArcGIS online: World Reference Overlay. Redlands, CA. Available online: http://www.arcgis.com/home/item.html?id=9763d83ba63048da8a2e0a71ccea4416

U.S. Geological Survey. 2014. *Frequently Asked Questions About the Landsat Missions.* U.S. Department of the Interior. June 19, 2014. Available online: http://landsat.usgs.gov/band_designations_landsat_satellites.php

Verma, K., R. K. Saxena, A. K. Barthwal and S. N. Deshmuch. 1994. Remote Sensing Technique for Mapping Salt Affected Soils. *International Journal of Remote Sensing*. Vol. 15, No. 9, pp. 1901-1914.

Weng, Y., P. Gong, and Z. Zhu. 2008. Soil Salt Content Estimation in the Yellow River Delta with Satellite Hyperspectral Data. *Canadian Journal of Remote Sensing*, Vol. 34, No. 3, pp. 259-270.

World Bank Climate Change Knowledge Portal. 2014. Average Monthly Temperature and Rainfall for Iran at Location *(31.17,56.03)* from 1990-2009. Climatic Research Unit (CRU) of University of East Anglia (UEA). Available Online: http://sdwebx.worldbank.org/climateportal/index.cfm

Yale. 2001. Unsupervised Classification Algorithms. August 15 2001. Available online: http://www.yale.edu/ceo/Projects/swap/landcover/Unsupervised_classification.html

Zarrineh, N., and M. Azari Najaf Abad. 2014. Integrated Water Resources Management in Iran: Environmental, Socio-economic and Political Review of Drought in Lake Urmia. *International Journal of Water Resources and Environmental Engineering.* Vol. 6, No. 1, pp. 40-48.

Zeinoddini, M., A. Bakhtiari, and M. Ehteshami. 2014. Long-term Impacts from Damming and Water Level Manipulation on Flow and Salinity Regimes in Lake Urmia, Iran. *Water and Environment Journal.* pp. 1-17.